SPECTRUM OF THE HYDROXYL RADICAL

by

COSMO CARLONE

B. Sc., University of Windsor, 1963

M. Sc., University of British Columbia, 1965

A THESIS SUBMITTED IN PARTIAL FULFILMENT OF

THE REQUIREMENTS FOR THE DEGREE OF

DOCTOR OF PHILOSOPHY

in the Department

of

PHYSICS

We accept this thesis as conforming to the

required standard

THE UNIVERSITY OF BRITISH COLUMBIA

March 1969

In presenting this thesis in partial fulfilment of the requirements for an advanced degree at the University of British Columbia, I agree that the Library shall make it freely available for reference and Study. I further agree that permission for extensive copying of this thesis for scholarly purposes may be granted by the Head of my Department or by his representatives. It is understood that copying or publication of this thesis for financial gain shall not be allowed without my written permission.

Department of Physics

The University of British Columbia
Vancouver 8, Canada

Date March 25, 1969

ACKNOWLEDGMENT

I wish to thank Professor F. W. Dalby for suggesting the problem and for constant supervision.

This work was supported by the National Research Council of Canada.

ABSTRACT

The $B^2\Sigma^+ \rightarrow A^2\Sigma^+$ and $C^2\Sigma^+ \rightarrow A^2\Sigma^+$ systems of OH and OD were photographed at high resolution. The apparent dissociation energy $D^o(A^2\Sigma^+)$ is calculated to be (18847 ± 15) cm^{-1} for OH and (19263 ± 15) cm^{-1} for OD. An upper limit to $D^o(X^2\Pi_{3/2})$ of OH is deduced to be (35420 ± 15) cm^{-1}. Evidence for a dispersion hump in the $B(^2\Sigma^+)$ state which is about 100 cm^{-1} larger than the hump in the $A(^2\Sigma^+)$ state is presented.

The broadening of the rotational lines in several bands of both systems has established a strong predissociation of the $A(^2\Sigma^+)$ state near v = 5 in OH. The lifetime of these predissociated levels is $\approx 10^{-11}$ seconds. A definite identification of the predissociating state has not been possible.

Newly discovered vibrational levels in the $C(^2\Sigma^+)$ state have led to the following constants, in cm^{-1}, of the OH radical in the $C^2\Sigma^+$ state

T_e	= 89500	B_e	= 4.247
D^o	= 29418 ± 15	α_e	= 0.078
ω_e	= 1232.9	γ (v=0)	= 1.09
$\omega_e x_e$	= 19.1	γ (v=1)	= 0.88

Rotational constants and spin splitting constants in the $A(^2\Sigma^+)$ and $B(^2\Sigma^+)$ states, more accurate than previously available are presented.

TABLE OF CONTENTS

		PAGE
LIST OF TABLES	. . . . .	v
LIST OF FIGURES	. . . . .	vi
LIST OF PLATES	. . . . .	vii
CHAPTER I -	INTRODUCTION.	1
II -	BASIC THEORY OF DIATOMIC MOLECULES. . . .	7
	(a) General theory	7
	(b) Application of the theory.	13
III -	EXPERIMENTAL.	20
IV -	RAW DATA.	25
V -	SPIN SPLITTING.	48
VI -	ROTATIONAL CONSTANTS.	56
VII -	DISPERSION HUMPS AND DISSOCIATION ENERGY.	61
	(a) $\triangle G(v + \frac{1}{2})$ of $A^2\Sigma^+$	61
	(b) Dissociation Energy of $A^2\Sigma^+$ state.	61
	(c) Energy levels	68
	(d) Dissociation Energy of $B^2\Sigma^+$ state .	72
	(e) Discussion.	76
VIII -	VIBRATIONAL CONSTANTS OF C, B STATES. .	78
IX -	PREDISSOCIATIONS IN $A^2\Sigma^+$ STATE. . . .	83
	(a) Gaydon predissociation.	83
	(b) Strong Predissociation.	85
	(c) Reconciliation with theory.	91

PAGE

X - THE $C^2\Sigma^+ \rightarrow B^2\Sigma^+$ SYSTEM 96

XI - WHAT NOW OH? 98

BIBLIOGRAPHY 102

APPENDIX I - Isotopic constant. 105

II - Computer program 106

III - Zero point Energy. 110

IV - Thermal and Pressure Broadening. 111

V - Predissociation by Rotation in $A^2\Sigma^+$ state of OD 113

VI - Electronic Isotope Shifts. 114

LIST OF TABLES

PAGE

TABLE

1 - Wavenumbers of the B → A system 26

2 - Wavenumbers of the C → A system 33

3 - Combination relations for the B state of OH . . 34

4 - Combination relations for the B state of OD . . 35

5 - Combination relations for the A state of OH . . 37

6 - Combination relations for the v = 4 level of the A state of OH 38

7 - Combination relations for the A state of OD . . 39

8 - Combination relations for the C state 41

9 - Band origins 42

10 - Spin splitting constants. 54

11 - Rotational constants. 59

12 - $\Delta G(v + \frac{1}{2})$ of A state of OH 63

13 - $\Delta G(v + \frac{1}{2})$ of A state of OD 64

14 - Energy of the vibrational levels. 69

15 - Wavenumbers of the (0,0) transition of the C → B system of OH 97

LIST OF FIGURES

FIGURE PAGE

1 - Structure of a $^2\Sigma^+ \rightarrow {}^2\Sigma^+$ transition 14

2 - Correlation of Ω with M_j of separated atoms. . . . 17

3 - Correlation of Ω with M_j of united atoms 18

4 - $^2\Pi$ state of OH. 19

5 - Apparatus 24

6 - $\Delta P(N)$ vs. N in C state of OH 53

7 - γ vs v in A state 55

8 - $\frac{\Delta_2 F}{N+\frac{1}{2}}$ vs $(N+\frac{1}{2})^2$ in v = 10 of A state of OD . 58

9 - Rotational constants vs v in A state 60

10 - $\Delta G(8.5)$ curve in A state of OH 62

11 - $\Delta G(v+\frac{1}{2})$ vs v in A state 65

12 - Atomic data and dissociation energy 71

13 - Limiting curve of dissociation in the B state . . . 75

14 - Observed bound states of the hydroxyl radical . . . 82

15 - Gaydon predissociation 84

16 - Predissociations in the A state 87

17 - Full width at half maximum in the (0,10) band of OD 88

18 - Variation of the full width at half maximum due to rotation 89

19 - Variation of the full width at half maximum due to vibration 90

LIST OF PLATES

PLATE PAGE

I - Three systems of the hydroxyl radical 44

II - The B→A system 45

III - The (0,7) and (0,8) transitions of the B→A system of OH 46

IV - The (0,9) and (0,12) transitions of the C→A system of OH and OD respectively. 47

CHAPTER I - INTRODUCTION

The hydroxyl radical (OH) is one of the more interesting molecules in nature. It is readily formed in combustion reactions where its spectrum is often used to determine the temperature of a flame (Dieke and Crosswhite, 1948). The OH emission has been detected in the upper atmosphere and is primarily responsible for the airglow (Meinel, 1950). Recently, the radio frequency transitions within the two lowest rotational states of the radical have been observed in astronomical sources (Barrett, 1968). Detection of the OH emission has usually been accompanied by exciting surprises. For example, it is almost certain that masing action is responsible for the radio signals of OH from outer space and the mechanism for the masing action is not yet understood. Detailed knowledge of the energy levels of the radical, which is the subject of this thesis, should help to solve the problems encountered with the OH emission.

This thesis contains a study of some of the electronic states of OH. All of these states have been studied previously but new vibrational levels and new transitions have been observed. The energy level diagram of OH can now be constructed very accurately up to 100,000 cm^{-1}

from the ground state. The assignment of the electronic and vibrational quantum numbers is unambiguously decided by the new transitions observed.

The emission spectrum of the radical was photographed at high resolution. The assuracy of the wavelengths measured is 10^{-3} Å, which is 10 times and in some cases 100 times better than the raw data previously available. The accuracy of the molecular constants in the states studied, such as internuclear separation and vibrational frequency, has been increased by a factor of 10.

One of the most useful constants of the molecule is the dissociation energy of the ground state. From a study of the $B^2\Sigma^+ \longrightarrow A^2\Sigma^+$ system, Barrow (1956) calculated the dissociation energy of the $A^2\Sigma^+$ state, the first excited state. He then determined the dissociation energy of the ground state to be (35450 ± 100) cm^{-1}. The $B^2\Sigma^+ \longrightarrow A^2\Sigma^+$ system of deutroxyl radical (OD) has been extended to include transitions to vibrational levels near the dissociation limit of the $A^2\Sigma^+$ state. The estimate of the error of the dissociation energy of the $A^2\Sigma^+$ state has been reduced by a factor of seven or better. The same error is transferred in calculating the dissociation energy of the ground state.

The increase in accuracy of the dissociation energies of the excited states has made possible the detection of dipole-dipole and higher order multipole interaction between the neutral hydrogen and oxygen atoms in the excited states. The net effect of this interaction was found to be repulsive and occurs at an internuclear separation much larger than that at which valence forces are predominant.

The high dispersion at which the transitions were photographed revealed that some of the spectral lines are broad. This effect was first observed in one of the OD transitions, the (0,9) of the $B^2\Sigma^+ \rightarrow A^2\Sigma^+$ system, by Bruce Nodwell in the summer of 1964, then an undergraduate research student for Professor Dalby. He, however, did not see the same effect in OH, in fact, he failed to observe the same transition in OH. The author subsequently constructed a source of OH which consistantly emitted the desired transitions with high intensity. The line broadening was seen in both the $B^2\Sigma^+ \rightarrow A^2\Sigma^+$ and $C^2\Sigma^+ \rightarrow A^2\Sigma^+$ systems of OH and OD. It became evident quite early that a predissociation occurs in the $A^2\Sigma^+$ state at high v's. The results were reported at the Conference of the Canadian Association of Physicists, held

at Calgary, Alberta, in June, 1968. Later on in the same year, a paper was discovered in the literature (Czarny and Felenbok, 1968) which reported line broadening in the same (0,9) band of OD and in the (0,6), (0,7) and (0,8) bands of OH. Our investigation is, however, much more comprehensive. In OD, the predissociation was detected from $v = 7$ through to $v = 13$ and in OH from $v = 5$ to $v = 7$. The sharp appearance of the transitions involving $v = 6$ in OD and $v = 4$ in OH is crucial in deciding where the predissociation is first noticeable. The dependence of the predissociation on the rotational quantum number was investigated in each vibrational level. Although much data has been collected on the predissociation, the theoretical explanation of the facts needs development.

Predissociations are interesting because the inverse process, pre-association, may be a very important step in the formation of molecules. When two atoms come together in a collision, they form a "quasi-molecule" at that separation for which valence forces are large. The quasi-molecule performs one vibration only for it has enough energy to break the bond. If energy is lost in that short time during which the vibration lasts (typically 10^{-13} seconds) a stable molecule is formed. The quasi-molecule can radiate to a lower closely lying vibrational

level. This transition lies in the far infra-red and is a slow process, $\approx 10^{-3}$ seconds. The quasi-molecule can also reach an excited state by pre-association and then radiate to the ground state. This transition lies in the optional region and is much faster, $\approx 10^{-8}$ seconds. Thus the probability of molecule formation is about 10^{-5} per collision by pre-association, but 10^{-10} by radiation to a lower vibrational level. For OH, the interest in pre-association is even greater because of the masing action observed in the OH radio frequency signal from outer space.

The $C^2\Sigma^+$ state is very deeply bound and high in excitation energy. The properties of this state have been determined from a study of the $C^2\Sigma^+ \rightarrow A^2\Sigma^+$ system and $C^2\Sigma^+ \rightarrow B^2\Sigma^+$ system. The former system has only been recently observed (Michel, 1957) and the latter is reported for the first time. The $C^2\Sigma^+$ state is not completely understood yet. The $C^2\Sigma^+ \rightarrow A^2\Sigma^+$ system of OH was extended to include transitions from a vibrational level lower in energy than the one previously thought to be v = 0 (Michel, 1957). The same system is reported for the first time in OD. The correct vibrational

numbering of the levels in the $C^2\Sigma^+$ state was deduced from the isotopic relations. The consequential new vibrational and rotational constants of the $C^2\Sigma^+$ state have been determined. A discussion of the electronic structure of the $C^2\Sigma^+$ state is also presented.

CHAPTER II - Basic Theory of Diatomic Molecules

In this chapter, the general theory of diatomic molecules is outlined in part (a) and the application of the theory to the determination of the molecular constants of the hydroxyl radical is given in part (b).

(a) General theory -

Molecular theory is based on the Born-Oppenheimer (1928) approximation according to which the total wave function of a molecular system is the product of electronic, vibrational and rotational terms. The approximation is good because the mass of the electron is much smaller than that of the nucleus.

In linear molecules, the classification of the electronic terms is based on the value of the component $\Lambda\hbar$ of the electronic angular momentum along the internuclear axis ($\hbar$ is Planck's constant divided by 2π). This is possible because there are no torques on the electron in the direction of the internuclear axis. The projection of the electronic angular momentum along the internuclear axis is conserved classically and Λ is therefore a good quantum number. For $\Lambda = 0, 1, 2, \ldots$ the electronic states are called $\Sigma, \Pi, \Delta, \cdots$. Although Λ is a good quantum number only in the non-rotating molecule, it is often found to be a good quantum number even in rotating molecules, to a good approximation.

The multiplicity of the electronic state is designated with an upper script on the left hand side and the projection of the total angular momentum on the internuclear axis is designated with a lower script on the right hand side, for example $^2\Pi_{3/2}$ $^2\Pi_{1/2}$.

The electronic wave function has a symmetry with respect to reflection at any plane passing through the two nuclei. For $\Lambda \neq 0$, the projection of the electronic angular momentum on the nuclear axis is $\pm \Lambda \hbar$. The degeneracy of these states is two-fold. For such degenerate states, a reflection of the electronic wave function at a plane passing through the nuclei can result in the same wave function or in the other wave function of opposite sign. States with $\Lambda \neq 0$ have therefore both symmetries but it is never expressed explicitly because the energy of both states is the same. For $\Lambda = 0$, the situation is different. A Σ^+ state reflects into itself at any plane passing through the nuclei, Σ^- goes into its negative, where the superscript denotes the symmetry with respect to reflection at a plane passing through the nuclei.

In the Born-Oppenheimer approximation, the eigenvalues of the electronic part of the wave function depend on the internuclear separation. Thus, when the electronic terms are eliminated from the Schroedinger equation for the molecule, there remains a term dependent on the internuclear separation, which together with internuclear Coulomb energy

can be interpreted as the potential energy of the nuclei in the field of the electrons. If this effective potential is called U(r), the Schroedinger equation for the nuclear terms reads

$$\text{(II-1)} \quad \left\{ -\frac{\hbar^2}{2\mu}\nabla^2 + U(r) \right\} \Psi = E\,\Psi$$

where μ is the reduced mass of the nuclei and ∇^2 is the Laplacean operator, with respect to the co-ordinates relative to the center of mass of the nuclei. Typical U(r) curves are illustrated in Figures 4, 14, 16. In the neighbourhood of the equilibrium internuclear distance r_e, U(r) can be expanded in a Taylor series,

$$\text{U(r)} = U(r_e+\xi) = U_e + \tfrac{1}{2}\mu\omega_e^2\xi^2 - a\xi^3 + b\xi^4 - \cdots$$

Expressing ∇^2 in spherical co-ordinates (r,θ,φ) and putting $\Psi = \frac{\chi(r)}{r}\,Y(\theta,\varphi)$, (II-1) becomes

$$\text{(II-2)} \begin{cases} -\frac{\hbar^2}{2\mu}\frac{d^2\chi}{d\xi^2}Y + \left(U_e + \tfrac{1}{2}\mu\omega_e^2\xi^2 - a\xi^3 + b\xi^4 - \cdots\right)\chi Y \\ + \frac{P^2}{2\mu r_e^2}\left(1 - \frac{2\xi}{r_e} + \frac{3\xi^2}{r_e^2} - \cdots\right)\chi Y = E\chi Y \end{cases}$$

where P^2 is the square of the angular momentum operator. Equation (II-2) describes the motion of a vib-rotor. The relative sizes of the terms in the expansions suggest solving

$$-\frac{\hbar^2}{2\mu}\chi'' + \left(U_e + \tfrac{1}{2}\mu\omega_e^2\xi^2\right)\chi = E_v\,\chi$$

which is the equation of the harmonic oscillator, and

$\frac{P^2}{2\mu r_e^2} Y = E_r Y$, which is the equation of a rigid rotor, and then treating the rest of the terms by perturbation theory. The energy values in cm^{-1}, are (Herzberg, 1950)

$$\frac{E(v,J)}{hc} = \omega_e(v+\tfrac{1}{2}) - \omega_e x_e (v+\tfrac{1}{2})^2 + \omega_e y_e (v+\tfrac{1}{2})^3 - \cdots$$
$$+ B_e J(J+1) - \alpha_e (v+\tfrac{1}{2}) J(J+1) - D_e J^2 (J+1)^2 + \cdots$$

where v = 0, 1, 2, ... is the vibrational quantum number.
J = 0, 1, 2, ... is the rotational quantum number.
and the constants are related to the shape of U(r).

The energy values are usually grouped differently,

$$\frac{E}{hc} = \omega_e(v+\tfrac{1}{2}) - \omega_e x_e (v+\tfrac{1}{2})^2 + \omega_e y_e (v+\tfrac{1}{2})^3 - \cdots$$
$$+ BJ(J+1) - DJ^2(J+1)^2 + HJ^3(J+1)^3 - \cdots \qquad \text{(II-3)}$$
$$= G(v) + F(J),$$

where it is understood that B, D, H are functions of v . Dunham (1932) has solved (II-2) for any U(r) that can be expanded in a Taylor series. For a fifteen term expansion of U(r) and with the Wentzel-Kramers-Brillouin perturbation method, Dunham found a term in the expression for the energy

which is independent of v and J and is

$$Y_{oo} = \frac{B_e}{4} + \frac{\alpha_e \omega_e}{12 B_e} + \frac{\alpha_e^2 \omega_e^2}{144 B_e^3} - \frac{\omega_e x_e}{4}$$

The selection rules for radiation are obtained in non-relativistic theory from the non-vanishing of the matrix element of the electric dipole moment, that is,

$$(II\text{-}4) \qquad \mathcal{M}_{12} = \langle \Lambda_1 v_1 J_1 | m | \Lambda_2 v_2 J_2 \rangle \neq 0$$

where m is the dipole moment. Since m is the component of a vector, the parity of the participating states must be opposite. From the properties of angular momentum we must have $\Delta J = 0, \pm 1$ (Landau and Lifshitz, 1965). Within the Born-Oppenheimer approximation, $\langle \Lambda_1 | \sum x_i + \sum y_i + \sum z_i | \Lambda_2 \rangle \neq 0$ if $\Delta \Lambda = 0, \pm 1$. ($x_i, y_i, z_i$ are the co-ordinates of the ith electron). If z is the direction of the internuclear axis, $\langle \Sigma^p | x | \Sigma^{p'} \rangle \neq 0$ only for $p = p'$ by a reflection through the xz plane. Similarly $\langle \Sigma^p | y | \Sigma^{p'} \rangle$ and $\langle \Sigma^p | z | \Sigma^{p'} \rangle \neq 0$ for $p = p'$ only ($p = \pm$).

The theory of radiationless transitions is not as well understood. We have not been able to explain the data on predissociations presented in Chapter IX by the present

theory. Since no photon is exchanged, the participating states must have the same parity and $\Delta J = 0$. It is assumed that transitions from the discreet levels of a bound state to those of an unbound state are brought about by terms in the Hamiltonian with the same symmetry character as $\underline{L}.\underline{S}$ or $\underline{J}.\underline{L}$ (Landau and Lifshitz, 1965). The selection rules can be derived from

(II-5a) $$\langle \Lambda_1 v_1 J_1 | \underline{L}\cdot\underline{S} | \Lambda_2 J_2 \rangle \neq 0$$

(II-5b) $$\langle \Lambda_1 v_1 J_1 | \underline{J}\cdot\underline{L} | \Lambda_2 J_2 \rangle \neq 0$$

where 1 refers to the bound state and 2 to the unbound state. Kovacs (1958) has discussed the matrix elements (II-5a). His results are given in Chapter IX. It is interesting to note that Herzberg (1950) states that for Σ states, only states of similar symmetry can interact, but Landau and Lifshitz (1965) state the opposite. Herzberg (1950) also states that the radiationless transition is a strong effect when the lifetime of the discreet level of $|\Lambda_1\rangle$ is of the order of 10^{-11} seconds or shorter. According to Herzberg (1950) a strong effect occurs when $\Delta S = 0$ and $\Delta\Lambda = 0, \pm 1$; for Σ states, the parity of the states must be the same. The lifetime of the predissociated levels of OH is shown in Chapter IX to be about 10^{-11} seconds, but the other conditions cannot possibly apply. Moreover, it is not obvious how these statements arise from condition (II-5).

(b) Application of the theory to the determination of the molecular constants of OH.

The ground state of the hydroxyl radical is $X\,^2\Pi$ (the Latin letter X serves to identify the lowest energy $^2\Pi$ state). Three bound excited states are known, $A^2\Sigma^+$, $B^2\Sigma^+$, $C^2\Sigma^+$. (A, B, C label excited states in order of energy). All measurements in this thesis come from a study of the $B^2\Sigma^+ \rightarrow A^2\Sigma^+$ and $C^2\Sigma^+ \rightarrow A^2\Sigma^+$ systems.

From the selection rules, the possible transitions of a $^2\Sigma^+ \rightarrow {}^2\Sigma^+$ system are as illustrated in Figure 1. N is the rotational quantum number, J is the total angular momentum. The parity of the levels is deduced from the facts that the spin function is independent of inversion, that the symmetry of the electronic wave function is given by p in Σ^p, that the vibrational wave function has no parity associated with it, and that the parity of the rotational wave function is given by the Spherical Harmonics. In Figure 1, the R branch for which $\Delta J = +1$ and the P branch for which $\Delta J = -1$ are much stronger than the Q branch for which $\Delta J = 0$. The line strengths are (Herzberg, 1950)

(II-6a) $$S_J^R = \frac{(J''+1)^2 - \frac{1}{4}}{J''+1}$$

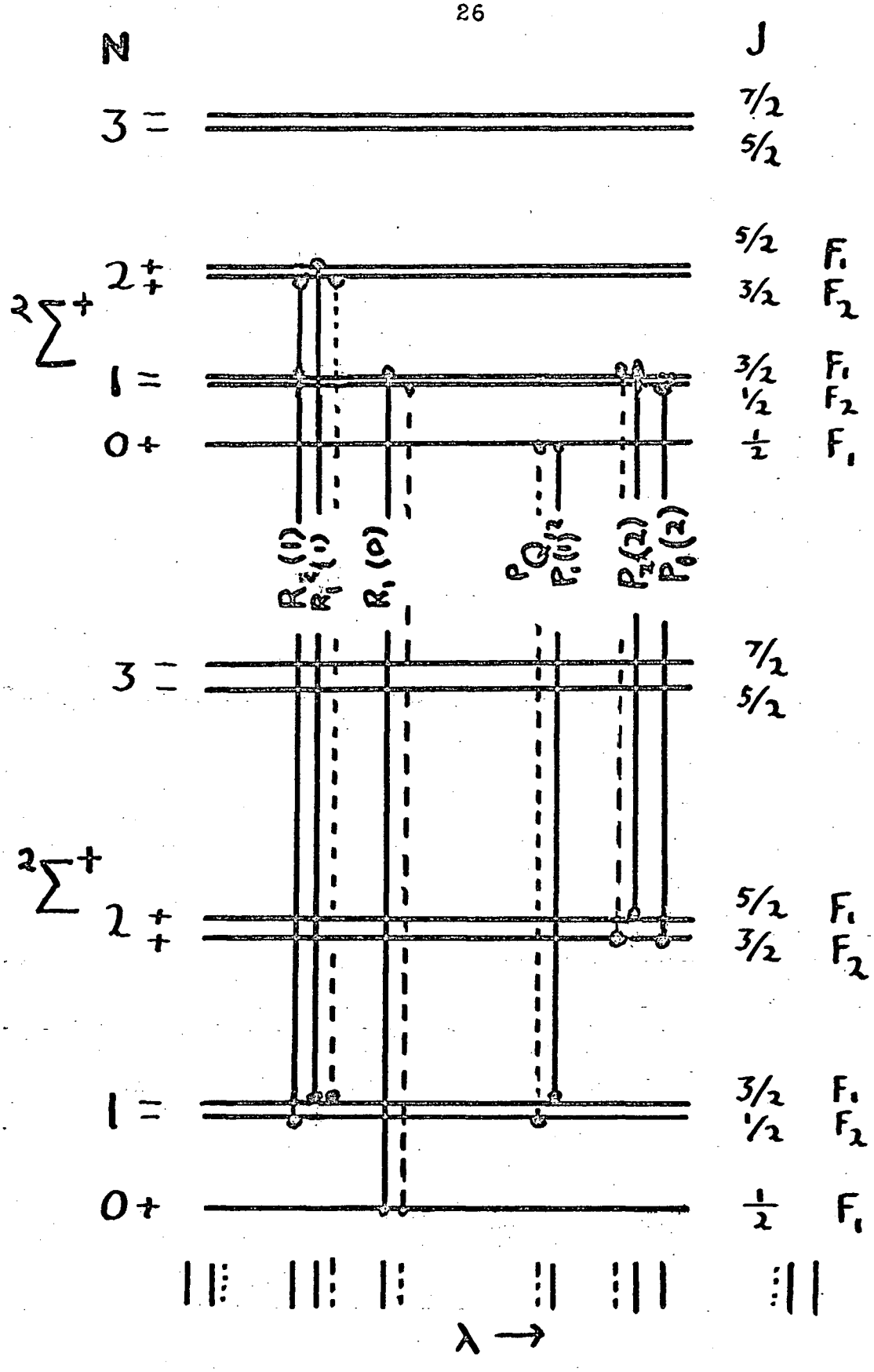

Figure 1. Structure of a $^2\Sigma^+ \rightarrow {}^2\Sigma^+$ transition.

(II-6b) $$S_J^Q = \frac{2J''+1}{4J''(J''+1)}$$

(II-6c) $$S_J^P = \frac{J''^2 - 1/4}{J''}$$

where the double prime refers to the lower state.

The directly observable quantities are the transitions R_1, R_2, Q_1, Q_2, P_1. P_2. Writing these transitions as the difference between energy levels, the molecular constants can be deduced. The results are quoted in Chapters V, VI, VII and VIII where the constants are evaluated.

The energy spacing between the levels with the same v but with rotational quantum numbers $N+1$ and $N-1$ is the combination relation $\Delta_2 F(N)$.

It is easily shown that

$$\frac{\Delta_2' F(N)}{N+\frac{1}{2}} = \frac{R(N)-P(N)}{N+\frac{1}{2}} = \left(4B'-6D'+\frac{27}{4}H'\right) + \left(-8D'+34H'\right)\left(N+\frac{1}{2}\right)^2 + 12H'\left(N+\frac{1}{2}\right)^4 + \cdots$$

where the single prime indicates upper electronic state constants. Similarly

$$\frac{\Delta_2'' F(N)}{N+\frac{1}{2}} = \frac{R(N-1)-P(N+1)}{N+\frac{1}{2}} = \quad \text{(same but with } '' \text{)}$$

gives lower electronic state constants. The numerical values of the combination relations provide a starting point for

labelling the quantum numbers associated with the transition.

In this thesis, the dissociation energy D° of the ground state $X\,^2\Pi$ is measured. D° is the difference between the energy of the lowest rotational level in in $X\,^2\Pi_{3/2}$ and the energy of the $X\,^2\Pi_{3/2}$ state for $r \longrightarrow \infty$. The $X\,^2\Pi_{3/2}$ state is assumed to result by dissociation in $O(^3P_2)+H(^2S)$. The correlation of molecular terms with the separated atoms and with the united atom is illustrated in Figures 2 and 3. In the Figures, Ω is the projection of the total angular momentum along the internuclear axis. In Figure 2, M_J is the sum of the magnetic numbers for the oxygen and hydrogen atoms simultaneously in a weak magnetic field. In Figure 3, M_J is the magnetic number of the fluorine atom in a weak magnetic field. The fine structure separation in Figures 2 and 3 are taken from Moore (1952). The OH potential wells as a function of internuclear distance are illustrated in Figure 4. The energy values in Figure 4 are taken from Dieke and Crosswhite (1948).

Referring to Figure 4, the shape of the potential function at large internuclear distances is not well known. It is shown in Chapter VII that there is a hump in the potential functions of the $B^2\Sigma^+$ states which is about 100 cm^{-1} larger than that in the $A^2\Sigma^+$ state. The origin of these forces is unknown but thought to be due to dispersive forces (London, 1937).

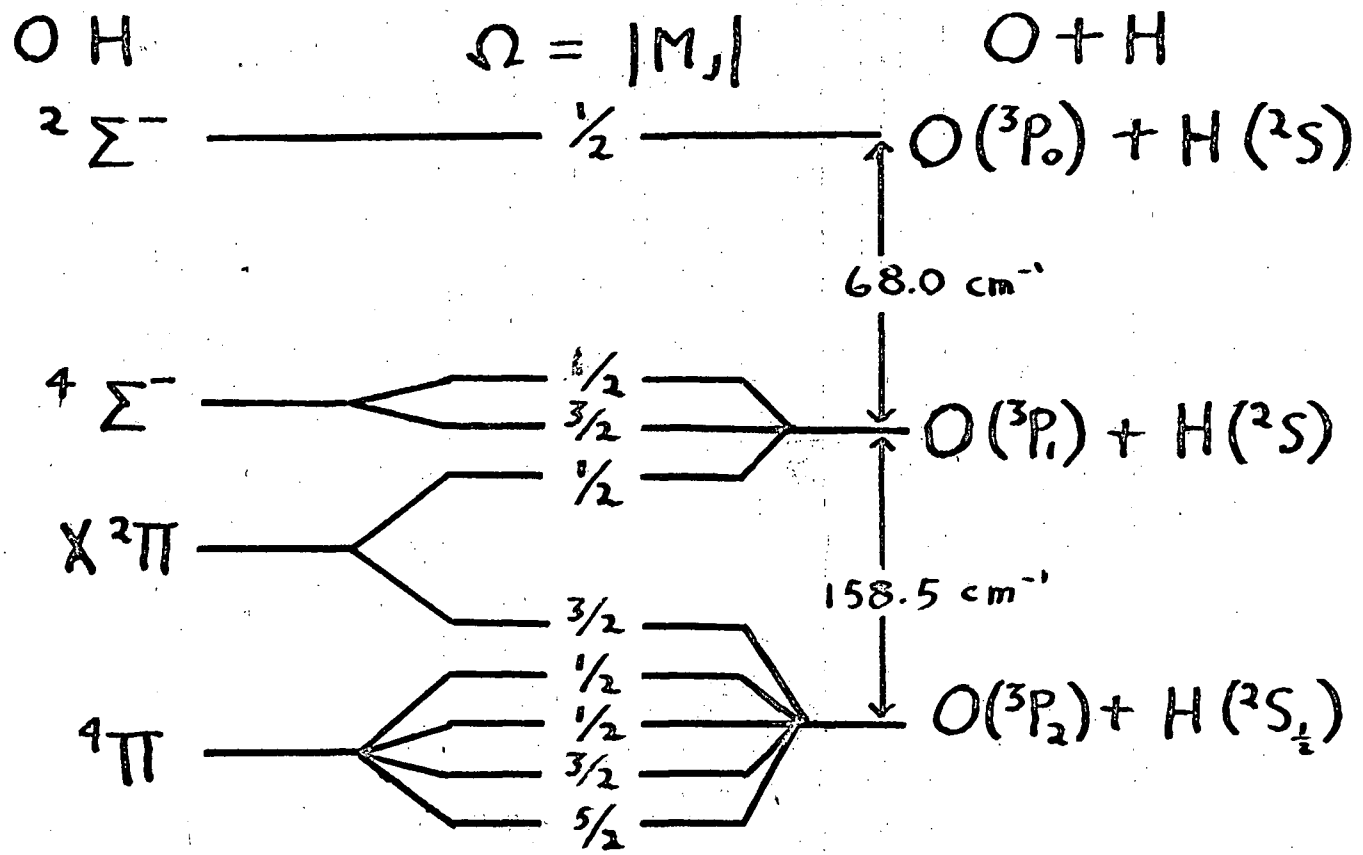

Figure 2. Schematic correlation of the molecular states of OH, including fine structure, with those of the separated atoms.

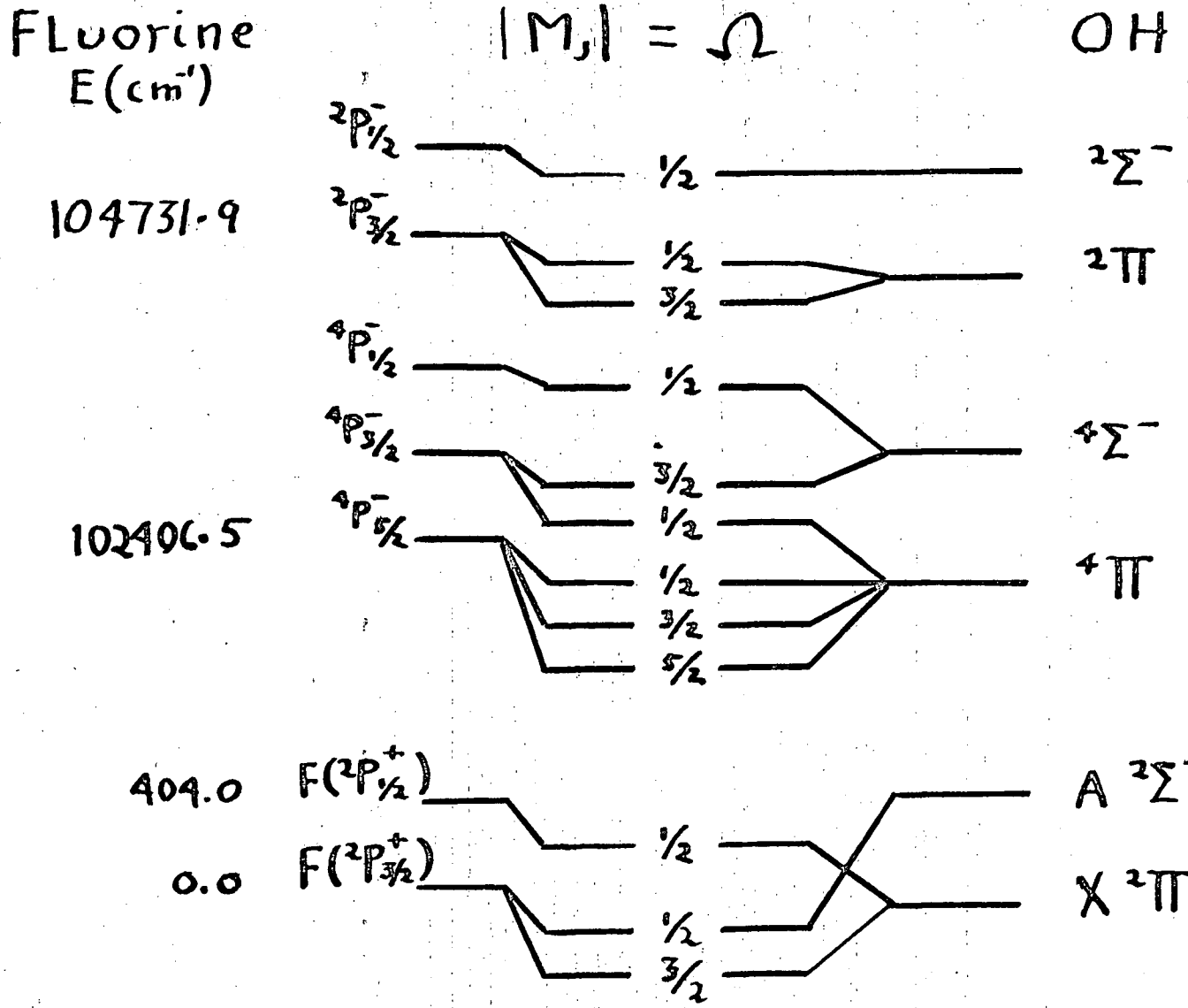

Figure 3. Schematic correlation of the molecular states of OH, including fine structure with those of the united atom.

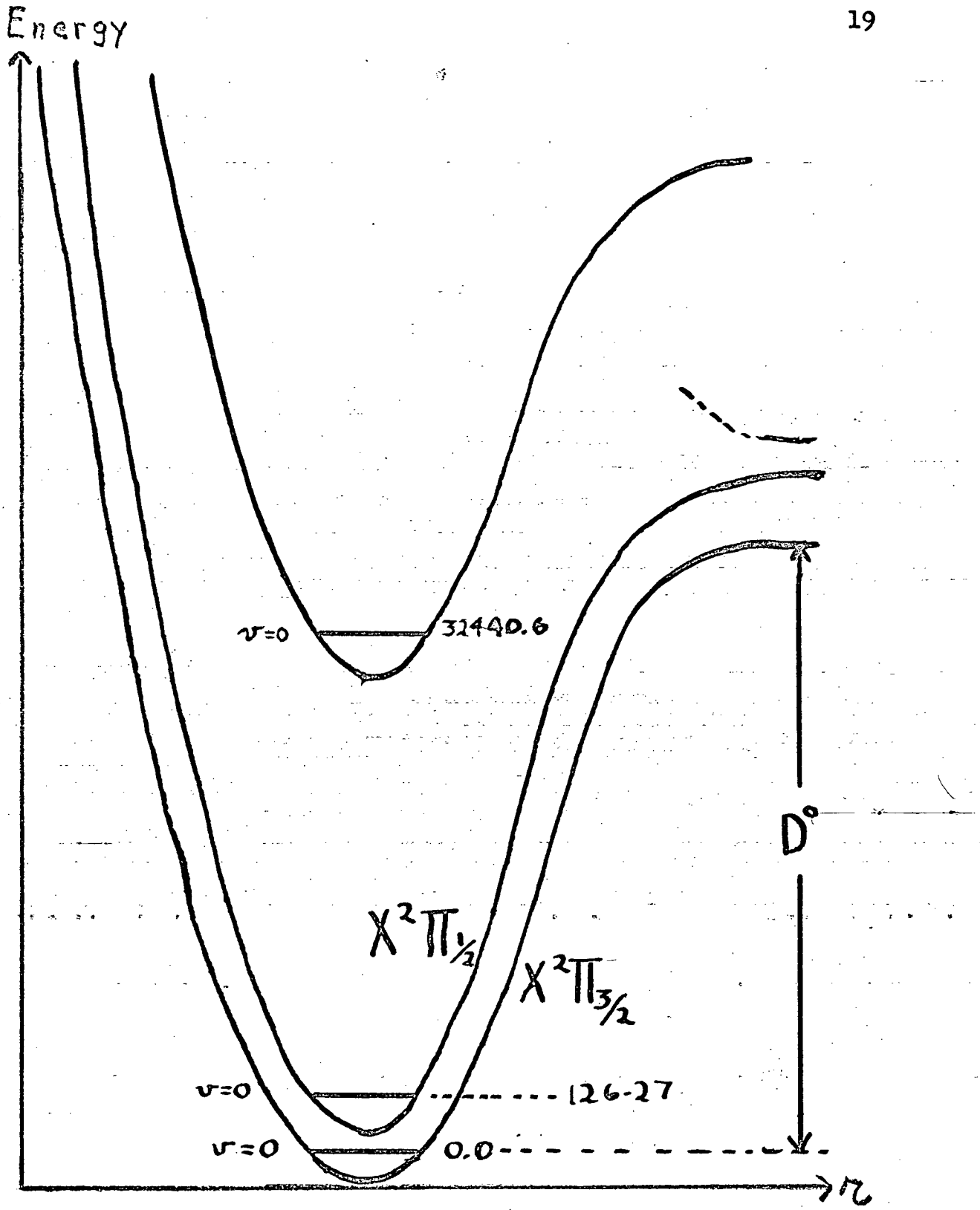

Figure 4. Correlation of molecular terms with atomic terms, including fine structure. The energy values are not to scale.

Chapter III - Experimental

The $B^2\Sigma^+ \longrightarrow A^2\Sigma^+$ and the $C^2\Sigma^+ \longrightarrow A^2\Sigma^+$ systems of the hydroxyl radical are much weaker than the well known $A^2\Sigma^+ \longrightarrow X^2\Pi$ system. See Plate I. It was found that a discharge through water vapour, as this vapour flowed rapidly through a hollow cathode produced the desired systems of OH quite strongly. The vacuum system was designed to achieve a fast pumping speed of the water vapour. The source of water was kept at 50° C, the vapour was then allowed to enter the vacuum system through a needle valve, and after traversing the discharge area, the vapour was collected by a liquid nitrogen trap of large area. The water vapour travelled a total distance of about 40 cm. All the flow tubes were 2.5 cm in diameter except for the aluminum hollow cathode which was 0.6 cm in diameter and 2.5 cm in length. A diffusion pump was used to bring about the fast pumping speed of all the gases formed in the discharge. A schematic diagram of the apparatus is shown in Fig. 5.

The power supply used delivered a maximum current of 200 milliamperes and is the amount of current utilized.

It was found that when the aluminum hollow cathode was clean, a bright red glow appeared in the hollow cathode area and the OH spectrum, as seen by a manual spectrograph, was very strong. As the discharge was maintained,

the glow became weaker and the discharge displaced itself away from the hollow cathode. Within a few hours, the glow in the hollow cathode and the OH spectrum were very much less intense. At the same time, the aluminum became covered with a rough black coating, presumably aluminum oxide. When this coating was removed with the help of a lathe and proper size drill and the hollow cathode put back in the vacuum system, a strong spectrum of OH was obtained again. The weakening of the spectrum due to the appearance of the coating on the hollow cathode limited the length of an exposure, which lasted from two to five hours.

The preliminary investigations of the spectrum were done on a Hilger medium quartz spectrograph, from which Plate I was made. Eventually, a Jarrell-Ash 3 · 4 meter Ebert spectrograph was used to photograph the regions from 2500 - 2800 Å in fourth order at a dispersion of 0.4 Å/mm, and from 3700 - 6500 Å in second order at a dispersion of 1 Å/mm. In the visible, the size of the plates covered only 500 Å for a given angle of the grating. Thus, the final measurements in this thesis come from 15 different exposures.

In photographing the far ultra-violet in fourth order, a chlorine lens was used to absorb the unwanted radiation at 3400 Å, which would have otherwise appeared in 3rd order.

The wavelength standards on the plates originated in an iron-neon hollow cathode. Typically over 100 well distributed standard lines were identified on each plate. The wavelength of these standards was taken from H.M. Cross-white's (1967) tabulation.

For wavelengths above 4800 Å, Kodak 103 a D plates were used and below 4800 Å, Kodak 103 a 0 plates were used.

The plates were read with the aid of a Grant comparator, with visual display (Tomkins and Fred, 1951) and digitalized output. As has already been mentioned, some of the lines appeared broad. The breadth of the lines was determined by measuring the observed full width at half maximum on the visual display of the line profile. Since density response calibration of the plates were not made, the measured half widths of the lines only approximately correspond to the true half-widths. Nevertheless, definite conclusions on the line breadths could be made, particularly those illustrated in Fig. 16, 17, 18.

The UBC IBM 7044 computer was used to fit dispersion curves to the standard wavelengths and then to interpolate from these curves the wavelength of the spectral lines originating in the OH discharge tube. The program used also converts the air wavelengths to wavenumbers, with the aid of Edlèn's formula for the change in the index of refraction of (dry) air at 15°C and 760 mm Hg (Coleman et al, 1960).

$$(III - 1) \quad n = 1 + 6432.8 \times 10^{-8} + \frac{2949810}{146 \times 10^{8} - \nu^{2}} + \frac{25540}{41 \times 10^{8} - \nu^{2}}$$

when ν is the vacuum wavenumber in cm^{-1}.

Appendix II gives the subroutine that fits the equation

$$(III - 2) \quad y = B(1) + B(2)x + \ldots + B(N + 1)x^{N}.$$

to several experimental points (x_i, y_i) , i = 1, NDATA. The B(N) of equation (III - 2) are not to be confused with the rotational B constants. The subroutine was used in several circumstances, for example in finding the relationship between $\Delta G (v + \frac{1}{2})$ and v in Fig. 10, and also in evaluating the spin splitting constants γ , whose plots are given in Fig. 6.

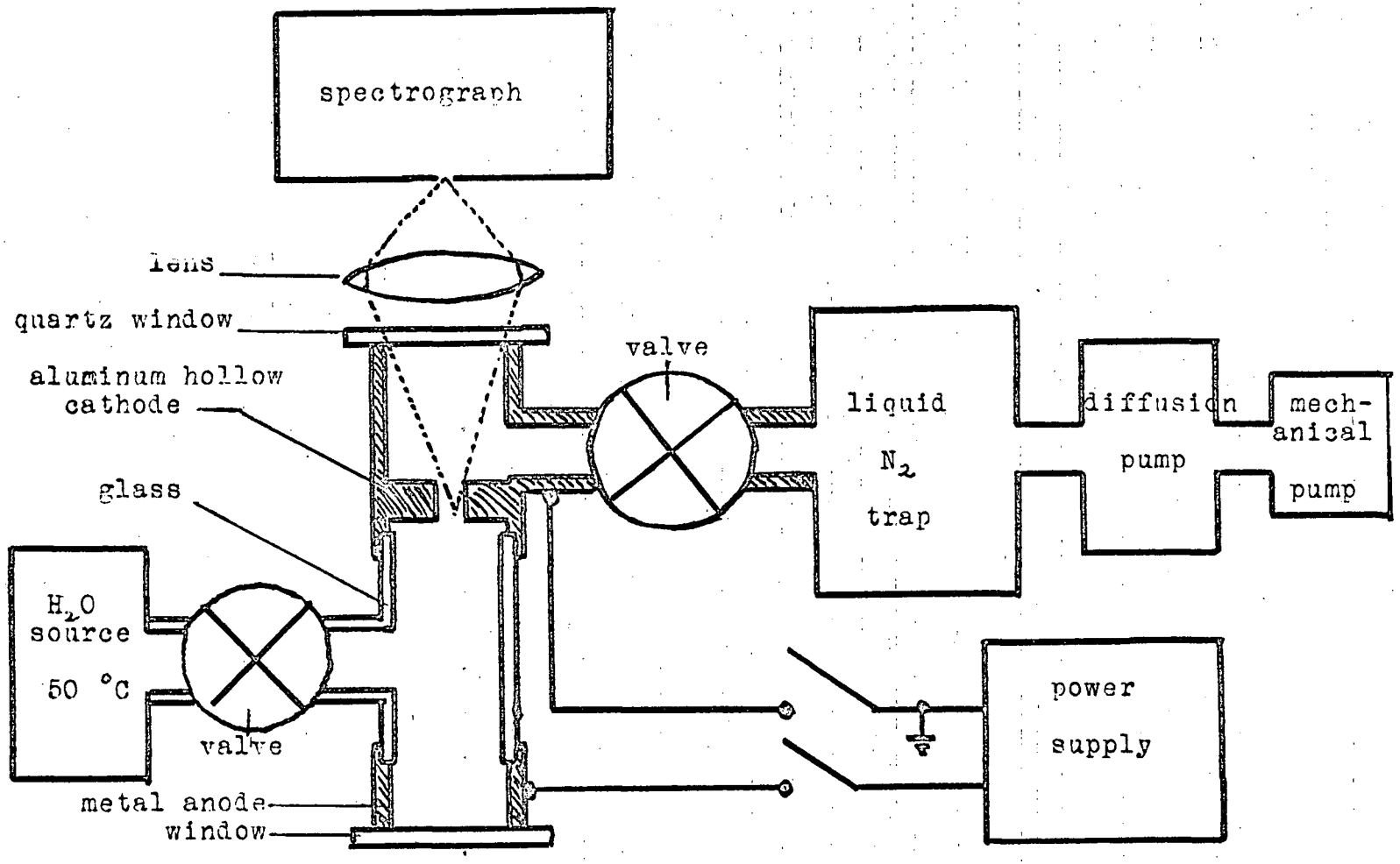

Figure 5. Schematic diagram of the apparatus.

Chapter IV - Raw Data

The wavenumbers of the spectral lines identified as transitions in the energy levels of OH and OD are given in tables 1 and 2. Proof of the identification of the transitions is given by the combination relations which are given in tables 3,4,5,6,7, and 8. Table 6 gives proof that the v numbering in the $A^2\Sigma^+$ state of OH is correct, that is, the $v = 4$ in the $A^2\Sigma^+$ state is the only one observed in both the $A \rightarrow X$ system and in the $B \rightarrow A$ system. The combination relations for this level as obtained from both systems agree with each other, as they should.

The three systems of OH and OD are shown on Plate I. The major part of the $B \rightarrow A$ system is shown on Plate II. The (0,7) and (0,8) transitions of the $B \rightarrow A$ system of OH are shown on Plate III. The (0,9) and (0,12) transitions in OH and OD respectively of the $C \rightarrow A$ system are shown on Plate IV.

The band origins of the bands photographed are given in table 9. ν_o, the band origin of a $^2\Sigma \rightarrow {}^2\Sigma$ transition is the energy difference between $J = \frac{1}{2}$ and $J = \frac{1}{2}$.

N	R_2	R_1	P_2	P_1
		(1,9)		
0	18058.76			
1	18063.57	18063.30	18038.72	
2	18064.76	18064.30	18024.05	18023.57
3	18062.59	18062.00	18006.05	18005.42
4	18057.54	18056.80	17985.60	17984.79
5	18050.14	18049.18	17963.43	17962.45
6	18041.14	18039.99	17940.66	17939.44
7	18031.72	18030.24	17918.62	17917.25
8	18021.44	18019.80	17899.87	17898.38
		(0,8)		
0	18238.46			
1	18242.14		18211.56	
2	18239.50	18239.21	18188.80	18188.45
3	18230.53	18230.07	18159.67	18159.16
4	18215.53	18214.90	18124.67	18124.02
5	18194.81	18194.14	18084.20	18083.40
6	18168.94	18168.03	18038.81	18037.88
7	18138.48	18137.45	17989.15	17988.08
8	18104.29	18103.03	17935.88	17934.64
9	18067.22	18065.83		
		(0,7)		
0	19512.3			
1	19512.3		19481.9	
2	19502.5		19451.5	
3	19482.8		19411.9	
4	19453.3		19362.4	
5	19414.5	19413.9	19303.9	19303.1
6	19366.2		19236.2	19235.5
7	19309.2	19308.5	19160.1	19158.9
8	19243.1		19075.2	
		(0,6)		
0	21136.8			
1	21134.4		21103.8	
2	21119.3		21068.3	
3	21091.4		21020.4	
4	21051.0		20960.2	
5	20998.4	20997.8	20888.1	
6	20933.8	20932.8	20803.7	20802.6
7	20856.6	20856.1	20707.4	20706.6
8			20600.2	20598.8

Table 1. Wavenumbers in cm^{-1} of OH bands of the $B^2\Sigma^+ \rightarrow A^2\Sigma^+$ system.

N	R_2	R_1	P_2	P_1
		(1,6)		
0	21795.2			
1	21788.1			21763.2
2	21766.9			21726.1
3	21730.6			21674.1
4	21679.9			21607.6
5	21612.6			21527.1
6				21432.1
		(0,5)		
0	23048.5			
1	23047.2			23016.6
2				
3	22993.5			22922.9
4	22944.4			22853.6
5	22880.6			22769.6
6	22801.3			22671.8
				22559.7
		(1,5)		
0	23710.6			
1	23701.9			23676.8
2	23676.8			23635.4
3	23633.8			23577.2
4	23573.7			
5	23495.4			23409.3
6				23301.3
		(1,4)		
1	25862.40			25838.02
2	25832.88			25792.09
3	25784.36	25783.92	25727.77	25727.24
4	25716.78	25715.91	25644.65	25643.88
5			25542.86	25541.94

Table 1. Wavenumbers in cm^{-1} of OH bands of the $B^2\Sigma^+ \longrightarrow A^2\Sigma^+$ system.

N	R_2	R_1	P_2	P_1
		(2.13)		
1	18038.0		18026.3	
2	18039.9		18020.2	
3	18040.4		18014.2	
4			18004.9	
		(1,12)		
1	18114.4		18099.6	
2	18114.4		18090.1	
3	18111.6		18077.7	
4	18106.7		18062.9	
5	18099.6		18046.1	
6	18090.1		18027.1	
7	18078.1	18077.7	18006.0	
8	18066.0	18065.3	17985.1	17984.5
9	18051.9	18051.1	17962.1	17961.1
10	18036.7	18035.9		
		(0,11)		
1	18267.2		18250.3	
2	18265.4		18238.1	
3	18260.0		18221.8	
4	18251.2		18202.0	
5	18238.9		18179.0	
6	18223.6		18152.8	
7	18204.8		18123.2	
8	18183.4	18182.9	18091.0	
9	18159.0	18158.4	18056.3	18055.7
10	18132.2	18131.5	18019.2	17018.3
11	18103.1	18102.3	17979.8	17978.9
12	18072.2	18071.3		17938.0
13	18039.9	18038.8	17896.5	17895.5
14	18006.6	18005.4	17853.4	17852.3
15	17972.8	17971.6	17810.1	17809.0
16			17767.7	17766.0

Table 1. Wavenumbers in cm^{-1} of OD bands of the $B^2\Sigma^+ \longrightarrow A^2\Sigma^+$ system

N	R_2	R_1	P_2	P_1
		(1,11)		
0	18814.5			
1	18812.8			
2	18809.0		18784.2	
3	18801.0		18767.0	
4	18789.5		18745.4	
5	18773.1		18719.7	
6	18753.1		18690.9	
7	18729.2		18657.7	18657.1
8	18701.7		18620.9	18620.4
9	18670.6	18670.2	18580.9	18580.1
10	18636.1	18635.2	18537.6	18536.7
11	18598.2	18597.4	18491.4	18490.5
12	18557.4	18556.4	18442.6	18441.7
13	18513.9	18512.9	18391.6	18390.5
14	18467.9	18466.8	18338.0	18337.0
15	18419.7	18418.2	18284.2	18282.9
16			18228.8	18227.4
		(0,10)		
0	19190.33			
1	19190.83		19174.34	
2	19186.56		19158.89	
3	19177.11		19138.69	
4	19162.78		19113.57	
5	19143.89	19143.61	19083.91	19083.54
6	19120.23	19119.79	19049.37	19048.92
7	19091.95	19091.31	19010.33	19009.77
8	19058.99	19058.37	18966.85	18966.21
9	19021.73	19021.05	18919.09	18918.38
10	18980.29	18979.53	18867.26	18866.47
11	18934.83	18934.07	18811.55	18810.68
12	18885.58	18884.67	18752.19	18751.31
13	18832.78	18831.82	18689.43	18688.41
14	18776.69	18775.59	18623.63	18622.48
15	18717.65	18716.43	18554.95	18553.80
16	18655.96	18654.70	18483.96	18482.60
17	18592.00	18590.62	18410.90	18409.61
18	18526.45	18525.07	18336.44	18335.08
19	18459.63	18458.20		18261.35
20				18185.81
21			18109.58	18107.71

Table 1. Wavenumbers in cm^{-1} of OD bands of the $B^2\Sigma^+ \longrightarrow A^2\Sigma^+$ system.

N	R_2	R_1	P_2	P_1
		(0,9)		
0		20307.9		
1		20307.4	20290.9	
2		20300.7	20273.3	
3		20288.1	20249.7	
4		20269.4	20220.2	
5		20244.8	20184.7	
6		20214.3	20143.6	20143.3
7		20178.2	20096.7	20096.2
8	20136.2	20135.7	20044.0	20043.5
9	20088.4	20088.0	19985.8	19985.1
10	20035.3	20034.8	19922.3	19921.6
11	19976.7	19976.1	19853.7	19852.7
12	19912.5		19779.5	19778.5
13	19844.2	19843.3	19700.6	19699.8
14	19770.6	19769.1	19617.2	19616.2
15	19692.1	19691.2	19529.6	19528.2
16	19609.6	19608.2	19437.2	19436.1
17	19522.9	19521.8	19341.1	19339.9
18	19431.6	19430.2	19241.6	19240.0
19	19337.1	19335.6		19137.3
20			19033.2	19031.2
21			18924.8	18923.1
		(1,9)		
1		20852.5	20837.8	
2		20844.1	20819.6	
3		20828.9	20794.8	
4		20807.2	20763.5	
5		20778.8	20725.6	
6		20743.9	20681.4	20681.0
7	20702.5	20702.1	20630.5	
8	20654.4	20654.2		
9	20600.0	20599.4	20510.3	20509.6

Table I . Wavenumbers in cm^{-1} of OD bands of the $B^2\Sigma^+ \longrightarrow A^2\Sigma^+$ system.

N	R_2	R_1	P_2	P_1
		(0,8)		
0	21589.6			
1	21588.1		21571.7	
2	21582.4			
3	21564.0		21525.4	
4	21541.8		21492.8	
5	21512.3		21452.1	
6	21476.4		21405.1	
7	21432.8		21351.3	
8			21291.0	
9	21326.6		21224.7	
10	21263.4		21150.3	
11	21194.4		21071.3	
12	21118.0		20985.0	
13	21036.4		20893.0	
14	20948.7	20947.8	20795.3	20795.0
15	20854.9		20692.3	20691.0
16	20755.3	20754.1		
17	20650.2	20648.9	20469.0	20467.7
18	20539.6	20538.2	20349.7	20348.2
19	20424.1	20422.5		20224.0
20	20303.3	20301.7		20095.2
21			19963.6	19961.9
22			19775.7	19774.3

K	R	P	R	P
	(1,8)		(1,7)	
0	22135.3			
1	22133.5	22119.0		
2	22123.4	22098.7	23547.5	
3	22105.2	22071.1	23528.8	23494.8
4	22079.4	22036.0	23498.9	23456.3
5	22046.2	21993.2	23462.6	23409.5
6	22005.7	21943.1	23416.6	23354.3
7	21957.2	21885.3	23362.6	23290.3
8	21901.3	21820.7	23300.4	23219.5
9	21837.8	21748.4	23229.6	23139.2
10			23150.0	
11			23061.4	22955.0

	(2,7)	
0	23920.5	
1	23915.1	23903.5
2	23899.8	23880.6
3	23874.6	23848.3
4	23839.4	23806.8
5	23795.4	23755.2
6	23740.8	23694.5
7	23676.1	23623.3
8		23543.4
9		23452.7

Table 1. Wavenumbers in cm^{-1} of OD bands of the $B^2\Sigma^+ \longrightarrow A^2\Sigma^+$ system.

N'	R_2	R_1	P_2	P_1
		(1.6)		
1	25118.41		25103.70	
2	25104.84		25080.48	
3	25082.08		25048.04	
4	25050.25	25050.04	25006.64	25006.32
5	25009.23	36008.80	24956.02	24955.58
6	24958.93	24958.36	24896.26	24895.74
7	24899.35	24898.76	24827.58	24826.84
8	24830.78	24829.98	24749.84	24749.08
9	24752.92	24752.21	24663.10	24662.26
10	24665.88	24665.28		

Table 1. Wavenumbers in cm^{-1} of OD bands of the $B^2\Sigma^+ \longrightarrow A^2\Sigma^+$ system.

N	R_1	R_2	P_1	P_2
		OH (0,9)		
0	37254.59			
1	37259.87	37257.90	37233.78	
2	37262.36	37259.14	37219.39	37218.13
3	37262.36	37257.90	37202.20	37200.08
4	37259.87	37254.59	37183.08	37179.98
5	37256.22	37250.09	37162.67	37158.74
6	37252.72	37245.67	37142.49	37137.65
7			37124.30	37118.57
8			37111.03	37104.38
		OH (1,9)		
0	38448.89			
1	38454.08	38451.82	38428.38	
2	38456.09	38453.30	38413.67	38412.78
3	38455.08	38451.82	38396.17	38394.56
4	38451.82	38447.61	38375.47	38374.14
5	38447.61	38442.62	38355.51	38352.38
6	38442.62	38437.24	38334.52	38330.80
7			38315.47	38310.98
		OH (1,8)		
0	39286.60			
1	39286.60	39284.95	39261.03	
2	39278.79	39276.00	39236.44	39235.47
3	39262.74	39259.23	39203.80	39202.15
4	39238.83	39234.73	39163.58	39161.12
5	39208.03	39202.94		39112.84
6			39062.15	39058.02
		OD (0,12)		
0	37378.7			
1	37381.6	37380.4	37367.1	
2	37380.4	37378.7	37357.2	
3	37376.5	37374.2	37444.9	37343.6
4	37369.9	37367.1	37329.2	37327.4
5	37360.9	37357.2	37310.9	37308.8
6			37290.4	37287.8
7			37268.3	37264.8
		OD (0,11)		
1	38079.5		38065.4	
2	38074.8	38073.1	38052.2	
3	38065.4	38063.4	38034.3	
4	38052.2	38049.3	38011.5	38009.6
5	38034.3	38030.5	38984.5	37982.2
6			37953.5	37950.7

Table 2. Wavenumbers of the $C\,^1\Sigma^- \rightarrow A\,^1\Sigma^+$ system.

OH v = 1 $B^2\Sigma^+$

N	1,9 $\Delta_2'F_1$	1,4 $\Delta_2'F_1$	1,9 $\Delta_2'F_2$	1,4 $\Delta_2'F_2$	1,6 $\Delta_2'F$	1,5 $\Delta_2'F$
1	24.49	24.38	24.73	24.38	24.9	25.1
2	40.74	40.79	40.73	40.79	40.8	41.4
3	56.59	56.69	56.56	56.59	56.5	56.7
4	72.01	72.13	71.94	72.03	72.3	
5	86.74		86.71		85.6	86.8
6	100.55		100.50			
7	113.00		113.06			
8	121.43		121.57			

OH v = 0 $B^2\Sigma^+$

N	0,8 $\Delta_2'F_1$	0,8 $\Delta_2'F_2$	0,7 $\Delta_2'F$	0,6 $\Delta_2'F$	0,5 $\Delta_2'F$
1	30.58	30.58	30.4	30.6	30.7
2	50.77	50.70	51.0	51.0	
3	70.90	70.84	70.9	71.0	70.6
4	90.82	90.86	90.9	90.8	90.7
5	110.73	110.62	110.7	110.0	111.0
6	130.16	130.16	130.0	130.1	129.5
7	149.38	149.33	149.4	149.4	
8	168.32	168.40	168.8		

Table 3. Combination relations in cm^{-1} for the $B^2\Sigma^+$ state of OH.

OD v = 2 $B\,^2\Sigma^+$

N	2,7 $\Delta_2'F$	2,13 $\Delta_2'F$
1	11.6	11.7
2	19.2	19.7
3	26.3	26.2
4	32.7	
5	40.3	
6	46.3	
7	52.8	

OD v = 1 $B\,^2\Sigma^+$

N	1,12 $\Delta_2'F_2$	1,11 $\Delta_2'F_2$	1,6 $\Delta_2'F_2$	1,12 $\Delta_2'F_1$	1,11 $\Delta_2'F_1$	1,6 $\Delta_2'F_1$
1	14.8		14.71	14.8	15.9	14.71
2	24.3	24.8	24.36	24.3	24.8	24.36
3	34.1	34.0	34.04	34.1	34.0	34.04
4	43.8	44.0	43.61	43.8	44.0	43.72
5	53.4	53.4	53.21	53.4	53.4	53.05
6	63.0	62.2	62.67	63.0	62.2	62.61
7	72.1	71.5	71.78	71.7	72.0	71.92
8	80.9	80.8	80.94	80.0	81.3	80.91
9	89.8	89.7	89.82	90.0	90.0	89.95
10		98.6			98.5	
11		106.8			107.0	
12		114.8			114.9	
13		122.3			122.4	
14		129.9			129.7	
15		135.5			135.3	

N	1,9 $\Delta_2'F$	1,8 Δ_2F	1,7 Δ_2F
1	14.7	14.5	
2	24.5	24.6	
3	34.0	34.1	34.0
4	43.7	43.4	42.6
5	53.2	53.0	53.1
6	62.6	62.6	62.2
7	71.6	71.9	72.2
8		80.6	80.9
9	89.7	89.4	90.3
10			
11			106.4

Table 4. Combination relations in cm^{-1} for the $B\,^2\Sigma^+$ state of OD.

OD v = 0 $B\,^2\Sigma^+$

N	0,11 $\Delta_2'F_2$	0,10 $\Delta_2'F_2$	0,9 $\Delta_2'F_2$	0,8 $\Delta_2'F_2$
1	16.9	16.31	16.5	16.3
2	27.3	27.67	27.4	
3	38.2	38.43	38.3	38.6
4	49.2	49.21	49.3	49.0
5	60.0	59.98	60.1	60.2
6	70.8	70.87	70.7	71.3
7	81.5	81.62	81.5	81.8
8	92.4	92.14	92.2	
9	102.7	102.64	102.6	101.9
10	113.0	113.03	113.0	113.1
11	123.3	123.28	123.0	123.2
12		133.40	133.0	132.9
13	143.4	143.36	143.6	143.4
14	153.2	153.06	153.3	153.4
15	162.7	162.74	162.5	162.6
16		172.04	172.4	
17		181.11	181.7	181.2
18		190.01	190.0	189.9

N	0,11 $\Delta_2'F_1$	0,10 $\Delta_2'F_1$	0,9 $\Delta_2'F_1$	0,8 $\Delta_2'F_1$
1	16.9	16.31	16.5	16.3
2	27.3	27.67	27.4	
3	38.2	38.43	38.4	38.6
4	49.2	49.21	49.3	49.0
5	60.0	60.07	60.1	60.2
6	70.8	70.86	71.0	71.3
7	81.5	81.55	82.0	81.8
8	91.9	92.16	92.1	
9	102.7	102.67	102.8	101.9
10	113.0	113.06	113.2	113.1
11	123.4	123.36	123.3	123.2
12	133.3	133.36		132.9
13	143.4	143.40	143.4	143.4
14	153.1	153.10	153.0	152.8
15	162.6	162.65	163.0	
16		172.01	172.1	
17		181.01	181.8	181.1
18		190.00	190.3	190.0
19			199.0	198.5

Table 4. Combination relations for the $B\,^2\Sigma^+$ state of OD.

OH v = 9 $A\,^2\Sigma^+$

	$\Delta_2''F_1$			$\Delta_2''F_2$		
	C → A		B → A	C → A		B → A
N	0,9	1,9	1,9	0,9	1,9	1,9
1	35.20	35.22	35.20	36.46	36.11	34.77
2	57.67	57.90	57.93	57.81	57.27	57.52
3	79.28	79.62	79.56	79.16	79.16	79.15
4	99.69	99.57	99.58	99.17	99.44	99.18
5	117.39	117.30	117.37	116.84	116.83	116.92
6	131.92	132.14	131.97	131.53	131.64	131.52
7	141.69		141.62	141.29		141.29

OH v = 8 $A\,^2\Sigma^+$

	$\Delta_2''F_1$	$\Delta_2''F_1$ - $\Delta_2'F_2$		$\Delta_2''F_2$
	C → A	B → A	C → A	B → A
N	1,8	0,8	1,8	0,8
1	50.16	50.03	51.14	49.65
2	82.80	82.98	82.80	82.46
3	115.22	115.17	114.88	114.85
4		146.64	146.40	146.32
5	176.68	176.70	176.71	176.73
6		206.05		205.65

	v = 7	v = 6		v = 5	
	B → A	B → A		B → A	
	$\Delta_2''F$	$\Delta_2''F$		$\Delta_2''F$	
N	0,7	0,6	1,6	0,5	1,5
1	60.8	68.5	69.1		75.2
2	100.4	114.0	114.1	124.3	124.2
3	140.1	159.1	159.3		
4	178.8	203.3	203.5	223.9	224.6
5	217.4	247.9	247.8	272.6	272.4
6	254.7	291.1		321.0	
7	291.0	334.3			

Table 5. Combination relations for the A state of OH.

	$B^2\Sigma^+ \rightarrow A^2\Sigma^+$		$A^2\Sigma^+ \rightarrow X^2\Pi$							
	$\Delta_2'' F_1$	$\Delta_2'' F_2$	$\Delta_2' F_1$				$\Delta_2' F_2$			
N	1,4	1,4	4,1	4,2	4,3	4,4	4,1	4,2	4,3	4,4
1	80.94	80.94	80.7	81.5	81.4	80.5	80.9	81.1	80.3	81.3
2	135.16	134.62	133.7	134.1	134.1	132.8	133.2	133.6	134.7	132.9
3	189.00	188.23	188.4	188.1	187.9	187.1	188.4	188.2	186.7	188.4
4	241.98	241.50	241.8	242.0	242.3	241.9	242.0	241.5	242.9	242.0

Table 6. Combination relations for the v = 4 level of the $A^2\Sigma^+$ state of OH, as obtained from the $A^2\Sigma^+ \rightarrow B^2\Sigma^+$ System and the $A^2\Sigma^+ \rightarrow X^2\Pi$ System (Tanaka and Koana, 1934).

OD v = 12 $A\,^2\Sigma^+$

N	$\Delta_2''F_2$ B → A 1,12	$\Delta_2''F_2$ C → A 0,12	$\Delta_2''F_1$ B → A 1,12	$\Delta_2''F_1$ C → A 0,12
1	21.6	21.5	21.6	21.5
2	36.7	36.8	36.7	36.6
3	51.5	51.3	51.5	51.2
4	65.5	65.4	65.5	65.6
5	79.5	80.3	79.5	79.5
6	93.5	92.4	93.5	92.6
7	104.9		105.6	
8	116.1		116.6	

OD v = 11 $A\,^2\Sigma^+$

N	$\Delta_2''F_2$ B → A 1,11	$\Delta_2''F_2$ B → A 0,11	$\Delta_2''F_2$ C → A 0,11	$\Delta_2''F_1$ B → A 1,11	$\Delta_2''F_1$ B → A 0,11	$\Delta_2''F_1$ C → A 0,11
1	30.3			30.3		
2	45.8	45.4	45.1	45.8	45.4	45.1
3	63.5	63.4	63.5	63.5	63.4	63.3
4	81.3	81.0	81.2	81.3	81.0	80.9
5	98.6	98.4	98.6	98.6	98.4	98.6
6	115.5	115.7		116.0	115.7	
7	132.2	132.6		132.7	132.6	
8	148.2	148.5		149.0	149.0	
9	164.1	164.3		165.0	164.5	
10	179.2	179.2		179.7	179.5	
11	193.5	1		193.6	193.4	
12	206.6	206.7		206.9	206.9	
13	219.4	218.8		219.4	219.0	
14	229.8	229.7		229.6	229.1	
15	239.1	239.2		239.4		

OD v = 6

N	$\Delta_2''F_2$ B → A 1,6	$\Delta_2''F_1$
2	70.37	
3	98.20	98.52
4	126.03	126.51
5	153.99	154.68
6	181.65	181.96
7	209.09	209.28
8	236.25	236.51

Table 7. Combination relations for the $A\,^2\Sigma^+$ state of OD.

	OD v = 10		OD v = 9			
	$\Delta_2''F_2$	$\Delta_2''F_1$	$\Delta_2''F_2$	$\Delta_2''F_1$	$\Delta_2''F_2$	$\Delta_2''F_1$
N	0,10	0,10	0,9	0,9	1,9	1,9
1	31.44		34.6		34.2	
2	52.19		57.7		57.6	
3	72.99		80.6		80.6	
4	93.20	93.57	103.3		103.3	
5	113.41	113.86	125.8	126.2	125.8	126.2
6	133.56	133.85	148.2	148.7	147.8	148.3
7	153.39	153.58	170.3	170.8		
8	172.86	172.93	192.3	193.1		192.4
9	191.73	191.90	213.9	214.1		
10	210.18	210.37	234.8	235.2		
11	228.10	228.22	255.8	256.3		
12	245.40	245.63	276.1	276.2		
13	261.95	262.19	295.2			
14	277.83	278.02	314.7	315.1		
15	292.73	292.99	333.3	333.1		
16	306.76	306.82	350.9	351.3		
17	319.52	319.62	368.0	368.2		
18		329.27		384.4		
19		339.26	398.4	399.0		
20	350.05	350.49		413.3		

	OD v = 8		OD v = 7	
	$\Delta_2'F_2$	$\Delta_2'F_1$	$\Delta_2''F$	$\Delta_2''F$	$\Delta_2''F$
N	0,8	0,8	1,8	1,7	2,7
1	62.7		36.5		39.8
2	62,7		62.4		66.7
3	86.8		87.3	91.2	93.0
4	111.1		112.0	119.3	119.5
5	136.7		136.3	144.4	143.9
6	161.0		160.9	172.5	172.1
7	185.4		185.0	197.1	197.5
8	208.1		208.8	223.3	223.4
9			232.6		
10	255.3				
11	278.4				
12	301.5				
13	322.8				
14	343.9	344.7			
15					
16	385.9				
17	405.6	405.8			
18		424.8			
19		443.6			
20		460.6			

Table 7. Combination relations for the $A^3\Sigma^+$ state of OD, obtained from the B → A system.

OH v = 0 $C\,^2\Sigma^+$

N	$\Delta_2' F_1$ 0,9	$\Delta_2' F_2$ 0,9
1	26.10	24.12
2	42.97	41.01
3	60.16	57.82
4	76.80	74.61
5	93.55	91.26
6	110.23	108.02

OH v = 1 $C\,^2\Sigma^+$

N	$\Delta_2' F_1$ 1,8	$\Delta_2' F_1$ 1,9	$\Delta_2' F_2$ 1,8	$\Delta_2' F_2$ 1,9
1	25.97	25.69	23.92	23.44
2	42.35	42.42	40.53	40.52
3	58.94	58.91	57.09	57.27
4	75.28	75.36	73.61	73.48
5		92.10	90.10	90.23
6		108.10		106.44

OD v = 0 $C\,^2\Sigma^+$

N	$\Delta_2' F_1$ 0,11	$\Delta_2' F_1$ 0,12	$\Delta_2' F_2$ 0,11	$\Delta_2' F_2$ 0,12
1	14.0	14.5	14.0	13.5
2	22.7	23.2	20.9	21.5
3	31.3	31.6	29.1	30.5
4	40.6	40.7	39.7	39.7
5	49.8	49.9	48.3	48.5

Table 8. Combination relations for the $C\,^2\Sigma^+$ state, both for OH and OD, as obtained from the C → A system.

OH B → A

v',v''	I	ν_0 (cm^{-1})	v',v''	I	ν_0 (cm^{-1})
0,8	8	18228.3	1,9	4	18050.5
0,7	8	19502.0	1,6	4	21786.5
0,6	6	21126.6	1,5	4	23702.1
0,5	4	23042.0	1,4	3	25864.9

OD B → A

v',v''	I	ν_0 (cm^{-1})	v',v''	I	ν_0 (cm^{-1})
0,11	9	18259.9	1,12	8	18017.0
0,10	10	19184.8	1,11	3	18806.6
0,9	10	20302.4	1,9	6	20849.3
0,8	10	21584.2	1,8	5	22131.4
2,13	2	18031.6	1,7	5	23558.9
2,7	4	23916.8	1,6	4	25127.6

OH C → A

v',v''	I	ν_0 (cm^{-1})	ν_0 (cm^{-1}) (Michel)
0,9	9	37245.9	
1,9	9	38440.5	
1,8	8	39277.9	39278.1
1,7			40551.6
3,7			42862.6
3,6			44450.9

OD C → A

v',v''	I	ν_0 (cm^{-1})
0,12	8	37374.8
0,11	8	38075.2

Table 9. Band origins of the bands photographed. The maximum intensity is taken arbitrarily at 10; the relative intensity is estimated by visual inspection of the plates.

CAPTIONS FOR PLATES

Plate I. The three systems of the hydroxyl radical (page 44).

Plate II. The B $\longrightarrow$ A system of the hydroxyl radical (page 45).

Plate III. The (0,8) and (0,7) transitions of the B $\longrightarrow$ A system in OH. The diffuse character of the (0,7) band shows a predissociation of the $A^2\Sigma^+$ state. In the (0,8) band the wavelengths of R(1) and P(5) are 5480 and 5528 Å respectively; in the (0,7) band the wavelengthe of R(1) and P(5) are 5124 and 5179 Å respectively. The two strong sharp lines between P(4) and R(7) in the (0,7) band are magnesium lines. (page 46)

Plate IV. Some bands of the C $\longrightarrow$ A system at high resolution. In the (0,12) band of OD, the wavelength of P(1) is 2675 Å and of P(7) is 2683 Å. (page 47)

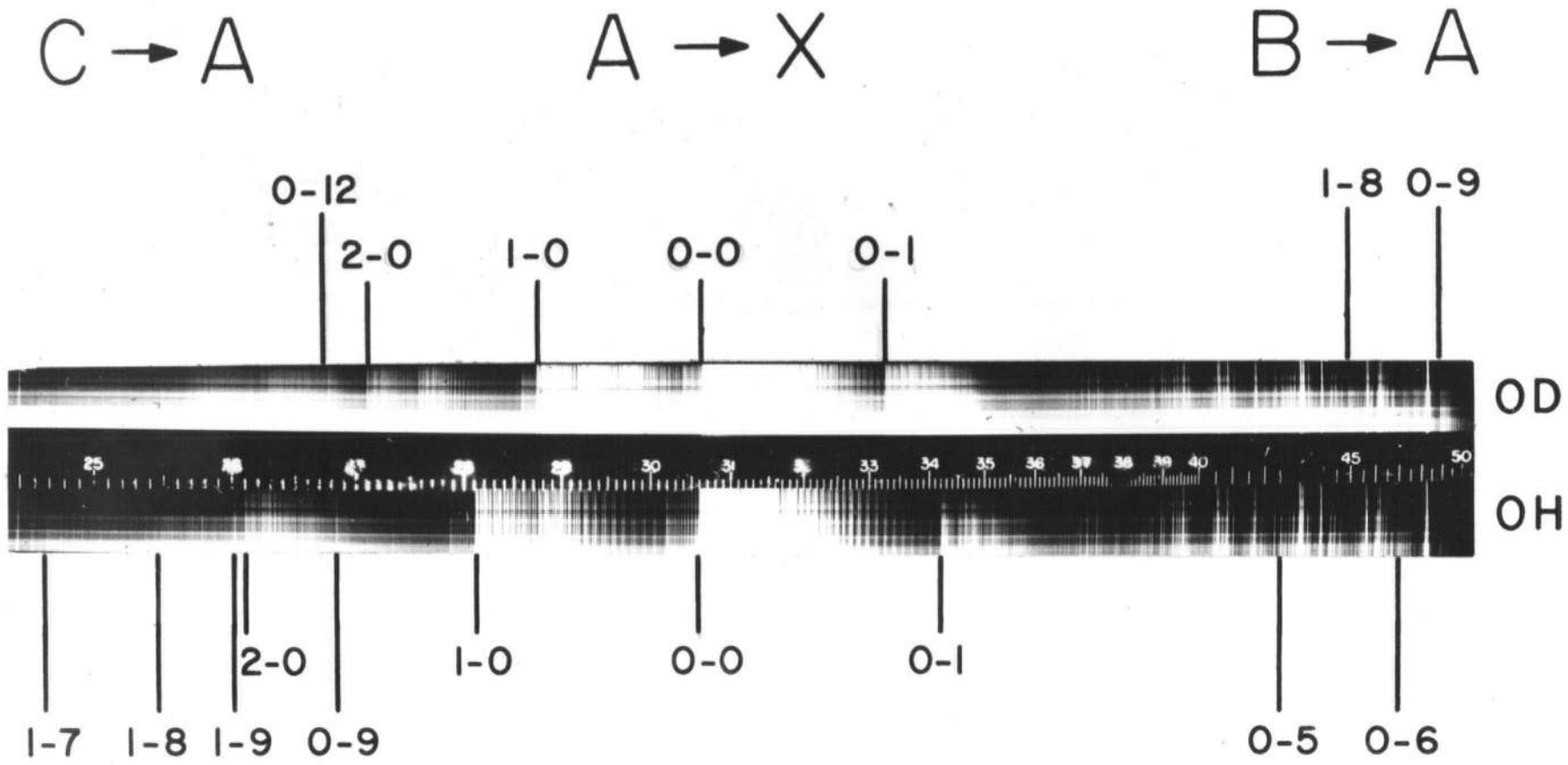
C → A
A → X
B → A
0-12
2-0
1-0
0-0
0-1
1-8
0-9
OD
OH
2-0
1-0
0-0
0-1
1-7
1-8
1-9
0-9
0-5
0-6

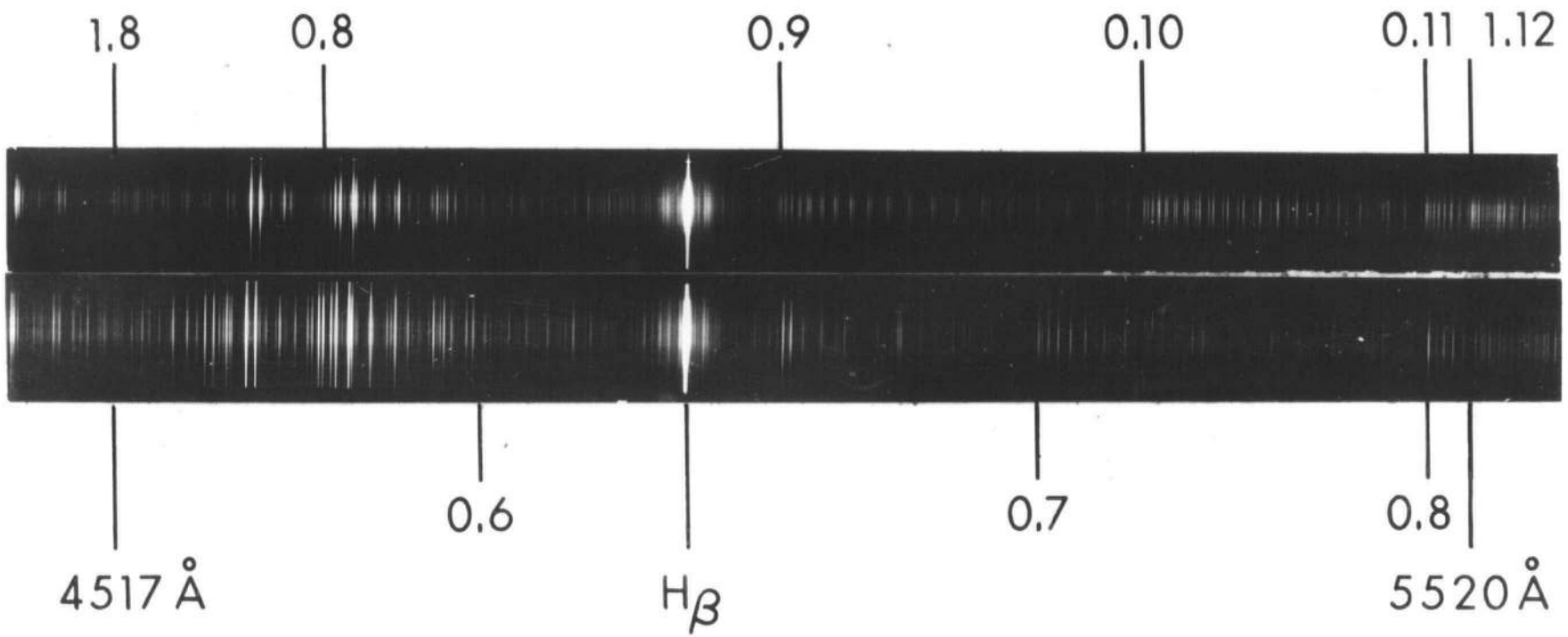
1.8
0.8
0.9
0.10
0.11
1.12
0.6
0.7
0.8
4517 Å
Hβ
5520 Å

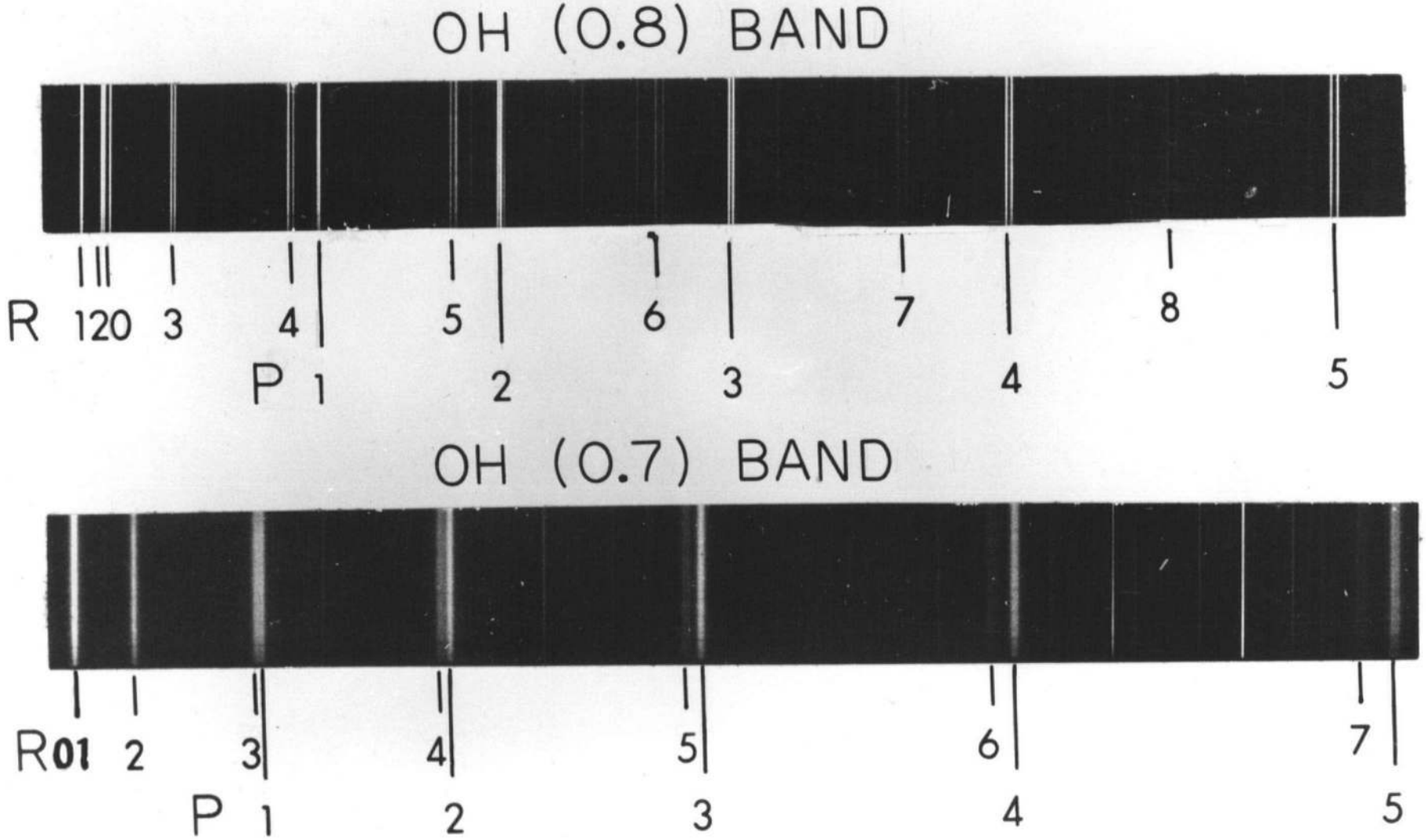
OH (0.8) BAND
R 120 3 4 5 6 7 8
P 1 2 3 4 5
OH (0.7) BAND
R01 2 3 4 5 6 7
P 1 2 3 4 5

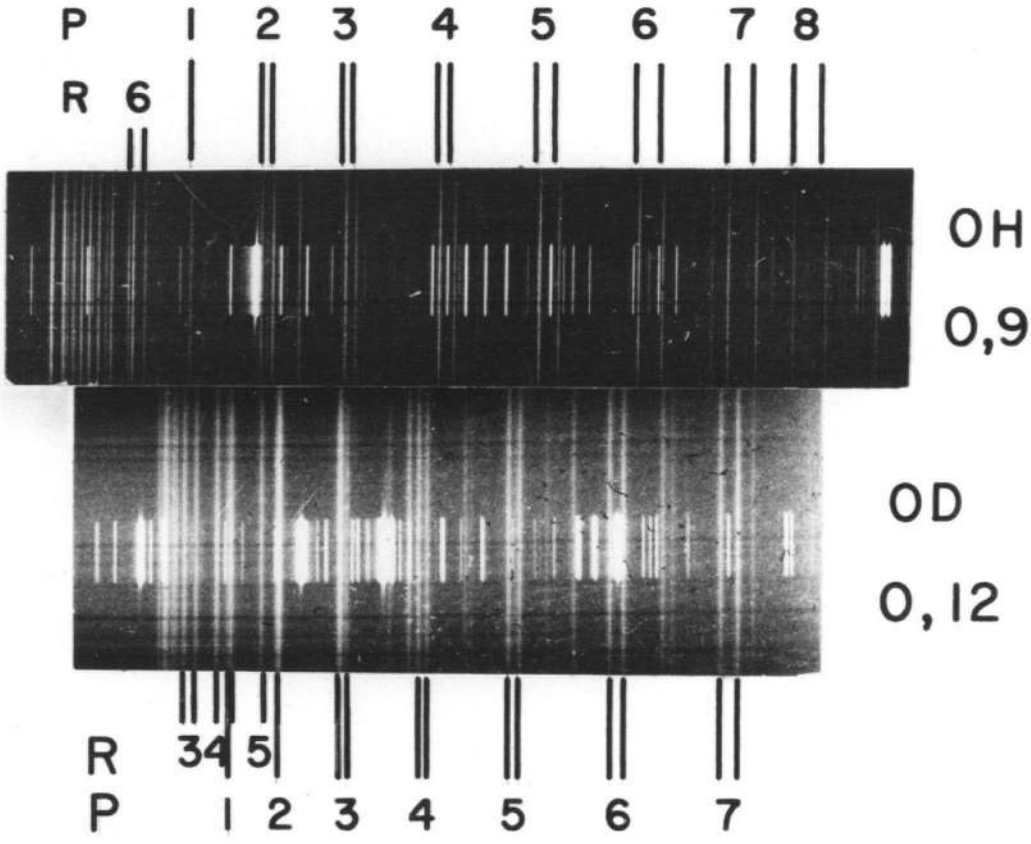
P 1 2 3 4 5 6 7 8
R 6
OH
0,9
OD
0,12
R 34 5
P 1 2 3 4 5 6 7

Chapter V - Spin splitting in the $C^2\Sigma^+$, $B^2\Sigma^+$, $A^2\Sigma^+$ states.

The spin splitting constant γ is calculated in this chapter for the C, B and A states. Contrary to the deduction by Czarny and Felenbok (1968) that γ changes sign in the A state, evidence is presented that it is positive throughout. The relative size of γ in each state is discussed.

The line strengths of the branches of a $^2\Sigma \rightarrow {}^2\Sigma$ have been given (II - 6). According to these formulas the P_1 and R_1 spin components have a greater intensity than the P_2 and R_2 components, the difference being more noticeable at low J''. This criterion was used to pick the R_1 and P_1 components from the R_2 and P_2 components in the (0,9) band of the $C \rightarrow A$ system of OH, where the intensity of the P_1 components is consistantly greater than that of the P_2 components. See Plate IV *. However in the (1,9) band of the $C \rightarrow A$ system of OH, the P_1 component is more intense than the P_2 component except in P (2) and P (3).

In the $B \rightarrow A$ system, the same conflicting evidence is found. In the (0,8) transition, discussed also by Czarny and Felenbok (1968), the R branch indicated that the shorter wavelength spin component has greater intensity. However,

---

* The R branch in the $C \rightarrow A$ bands reverses upon itself, with transitions often overlapped. Consequently, the information from the R branch is not as dependable.

P (2) and P (5) have the opposite pattern. Moreover, P (6) and R (4) have the longer wavelength spin component visibly perturbed, as they are much weaker than theoretically predicted. Equations (II - 8) represent poorly the intensity pattern observed both in the $C \rightarrow A$ and $B \rightarrow A$ systems. Fortunately another way was found which determined the sign of γ.*

In the (0,8) band of the $B \rightarrow A$ system of OH, the weak $^{P}Q_{12}(1)$ transition was found at the frequency predicted by the calculated value of γ for $v = 8$, but at higher frequency than P (1). This implies that in $v = 8$ of $A^2\Sigma^+$ $J = \frac{1}{2}$ is lower in energy than $J = {}^3/_2$ in the $N = 1$ level (Fig. 4) and hence γ is positive. Czarny and Felenbok also observed the same $^{P}Q_{12}(1)$ transition at higher frequency then P(1).

The (0,6) and (0,7) transitions in the $B \rightarrow A$ system of OH appeared broad and the spin components at low N's could not be resolved. However, at $N = 5, 6, 7$ the spin components were resolved and the splitting is comparable to

* The assignment of the spin component in (0,9) band of the $C \rightarrow A$ systems turns out to be the same as that already indicated.

that in (0,8), implying that the magnitude of γ has not changed very much. The nagnitude of γ in $v = 4$ is also large, as measured from the sharp (1,4) transition. Michel (1957) quotes γ in $v = 6$ to be -0.02, but he does not give the resolved spin components of the transitions from which the value of γ was calculated. Our results indicate that γ in $v = 6$ is ≈ 0.18 cm^{-1}. Unfortunately, no splitting in the (0,5) nor (1,5) transitions, both of which are broad, was observed. If there is a change in the sign of γ, which is unlikely, it would have to take place between $v = 4$ and $v = 6$. From the observation of the $^{P}Q_{12}(1)$ transition in $v = 8$, γ is positive in $v = 8$ and is probably positive throughout the A state as shown in Fig. 7. In order to make the combination relations for the A state from the $C \rightarrow A$ and $B \longrightarrow A$ systems agree with each other, the longer frequency components of the $C \rightarrow A$ transitions had to be associated with the F_1 levels. γ has the same sign in the C state as it does in the A state.

The relationship (Herzberg, 1950)

$$(V - 1) \quad P_1(N) - P_2(N) = (\gamma' - \gamma'') \; N - \tfrac{1}{2} \; (\gamma' + \gamma'')$$

is plotted in Fig. 6 for the (0,9), (1,9) and (1,8) bands of the $C \rightarrow A$ system of OH. By similar plots, the γ's

of most vibrational levels were obtained. The data from OD in the $C \rightarrow A$ system is less accurate because the lines are broad.

The spin splitting constant can also be calculated from the combination relations, that is, (Herzberg, 1950)

$$\Delta_2 F_1(N) - \Delta_2 F_2(N) = 2\gamma \qquad (V-2)$$

Equation (V - 2) gives very accurate values of γ in the C state because it is large in that state, and reasonably accurate values of γ in the A state.

All the measured spin splitting constants are given in table 10.

The variation of the spin-splitting constant is shown in Fig. 7. The minimum at high v's is real as is obvious from the different slopes of equation (V - 1) for the (1,8) and (1,9) bands of Fig. 6. According to Van Vleck (1929) the major contribution to the spin splitting in a $^2\Sigma$ state arises from the non-vanishing magnetic moment of the electronic angular momentum due to rotational distortion. This splitting is proportional to B/ν where B is the rotational constant and ν is the energy separation to the nearest $^2\Pi$ state. The experimental data at low v's bears out Van Vleck's theory, since

$$\frac{\gamma\ (v = 0,\ OD)}{\gamma\ (v = 0,\ OH)} = \frac{0.6}{1.09} = 0.55$$

$$\frac{\gamma\ (v = 0,\ OD)}{\gamma\ (v = 0,\ OH)} = \frac{0.13}{0.23} = 0.57$$

$$\frac{B_{(OD)}}{B(OH)} = \rho^2 = 0.53$$

Perhaps a more quantitative application of Van Vleck's theory can explain, not only the minimum observed in Fig. 7, but also the relative sizes of the γ in the A, B, and C, states. For example, in the A state, the B values decrease linearly up to $v = 5$ by 30% (Fig. 9); in the same range, γ decreases by 25%. In the C state, the B value decreases linearly in going from $v = 0$ to $v = 3$ by only 6%; in the same range, γ decreases non-linearly by 45%.

Figure 6. Spin splitting in the P branch of the C $\rightarrow$ A system of OH.

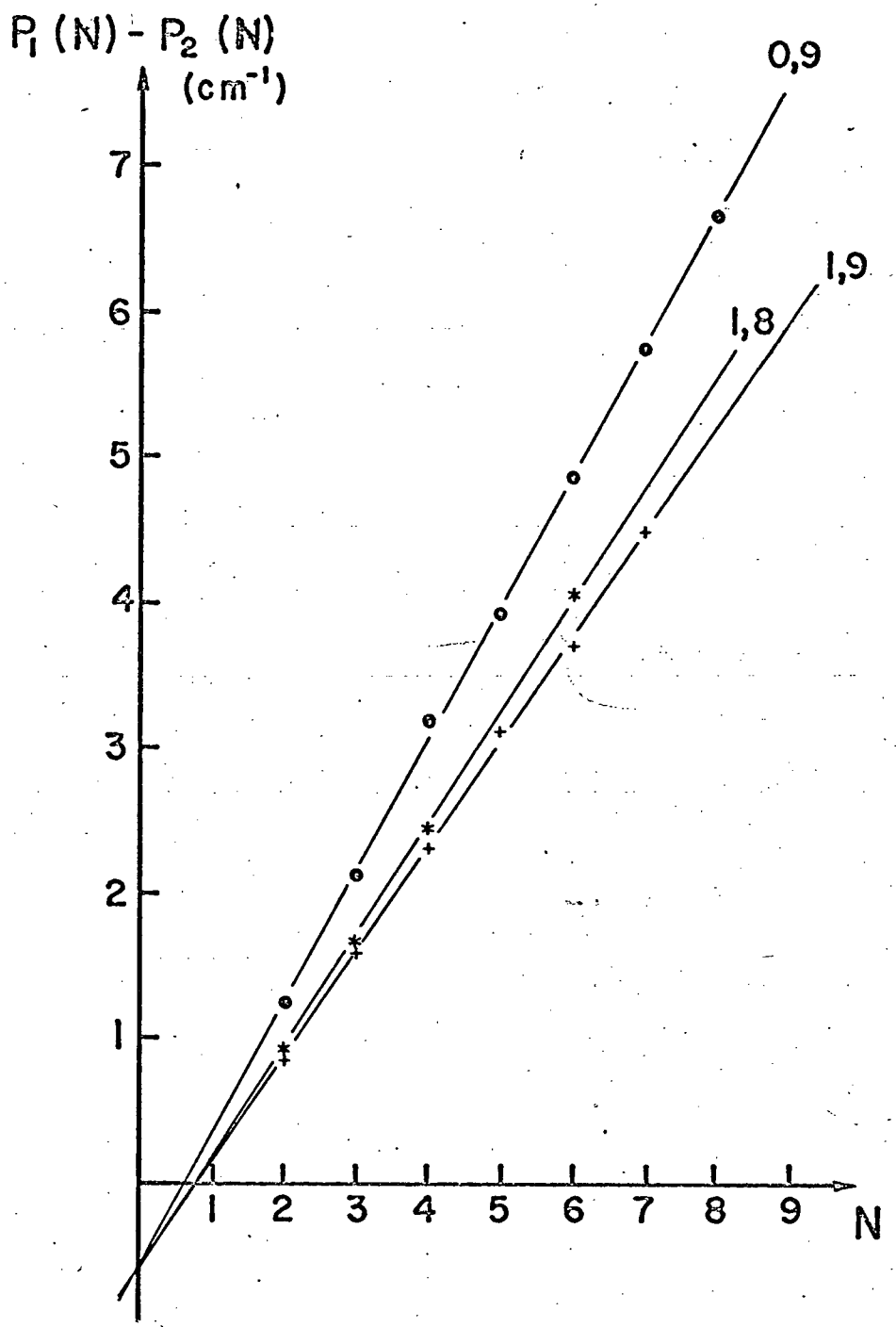

State	v	OH
C	3	a
	2	---
	1	0.88 [b]
	0	1.09
		C→A / B→A
	9	0.18 / 0.20
	8	0.16 / 0.16
	7	c
	6	c
	5	---
A	4	0.19
		A→X
	3	0.19 [d]
	2	0.20 [d]
	1	0.21 [d]
	0	0.22 [d]
B	1	< 0.03
	0	< 0.03

State	v	OD
C	0	0.6
		B→A
	12	0.11
	11	0.10
	10	0.08
	9	0.09
A	8	---
	7	---
	6	0.11
		A→X
	1	0.14 [e]
	0	0.08 [f]
B	1	< 0.05
	0	< 0.05

Table 10. Spin splittings constants, in cm^{-1}.

a. Michel's value is 0.67.
b. Michel's value is 0.87.
c. The lines of the (0,6) and (0,7) bands are broad and the spin components could not be resolved at low N. AT N = 5,6,7 the splittings observed were comparable to those in the (0,8) band, indicating that γ in v = 6 and 7 is comparable in magnitude to that in v = 8. See Fig. 7.
d. These are calculated from the data of Dieke and Crosswhite (1948)
e. Calculated from the data of Oura and Ninomiya (1943)
f. Calculated from the data of Ishaq (1937)

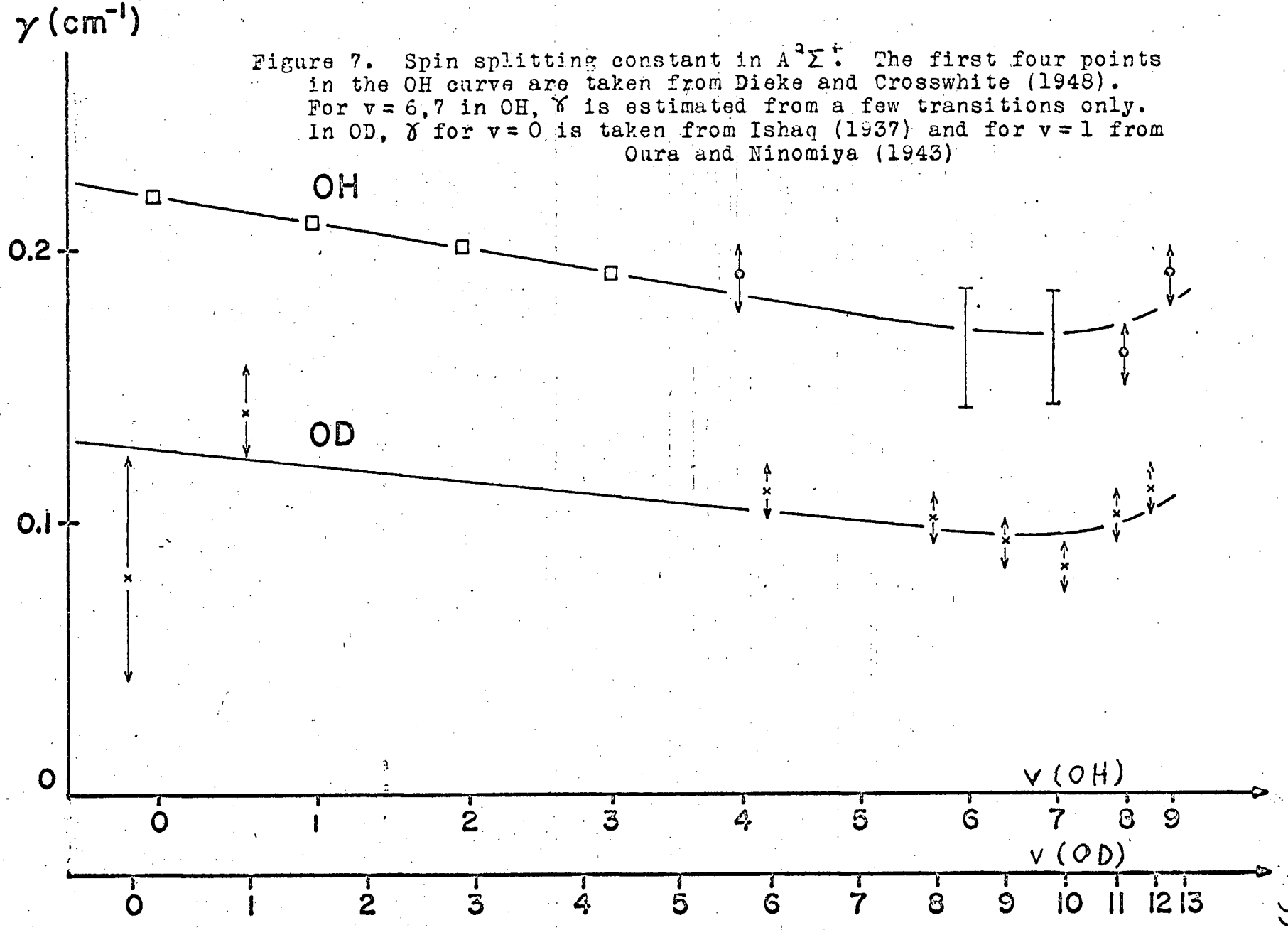

Figure 7. Spin splitting constant in $A^2\Sigma^+$. The first four points in the OH curve are taken from Dieke and Crosswhite (1948). For v = 6,7 in OH, γ is estimated from a few transitions only. In OD, γ for v = 0 is taken from Ishaq (1937) and for v = 1 from Oura and Ninomiya (1943)

Chapter VI - Rotational Constants in the $A^2\Sigma^+$, $B^2\Sigma^+$, $C^2\Sigma^+$ states.

The rotational constants are found from the relationship (Herzberg, 1950)

$$\text{(VI - 1)} \qquad \frac{\Delta_2 F_1 - \gamma}{N+\frac{1}{2}} = \frac{\Delta_2 F_2 + \gamma}{N+\frac{1}{2}} =$$

$$= (4B - 6D + \tfrac{27}{4}H) + (-8D + 34H)(N+\tfrac{1}{2})^2 + 12H(N+\tfrac{1}{2})^4$$

if γ is positive. Usually γ and H are so small that they are not included in the equation. The left hand side of equation (VI - 1), without the γ, is plotted against $(N + \frac{1}{2})^2$ in Fig. 8 for the $v = 10$ level of $A^2\Sigma^+$ of OD. It was found that even at low $(N + \frac{1}{2})^2$ values the correction due to the γ could not be noticed in the Figure. For the C state where γ is very large, it was found that the correction is demantatory in order to make any sense of the curves obtained. Fig. 8 shows the necessity of a three term expansion of the rotational energy in $v = 10$ of $A^2\Sigma^+$ of OD since the last six points deviate considerably from the straight line.

(VI - 2) $F(N) = BN(N+1) - DN^2(N+1)^2 + HN^3(N+1)^3$

The rotational constants of the A, B, and C states are given in table 11 and are plotted in Fig. 9.

Assuming that for the C state,

(VI - 3) $B_v = B_e - \alpha_e(v+\frac{1}{2})$

then $B_e = 4.247\ cm^{-1}$ and $\alpha_e = 0.078\ cm^{-1}$.

Testing the isotopic relations in the C state,

$$\frac{B_o(OD)}{B_o(OH)} = \frac{2.25}{4.213} = 0.534 \ ; \ \rho^2 = 0.529$$

The agreement is excellent. The B_e value of OH gives $r_e = 2.048$ Å.

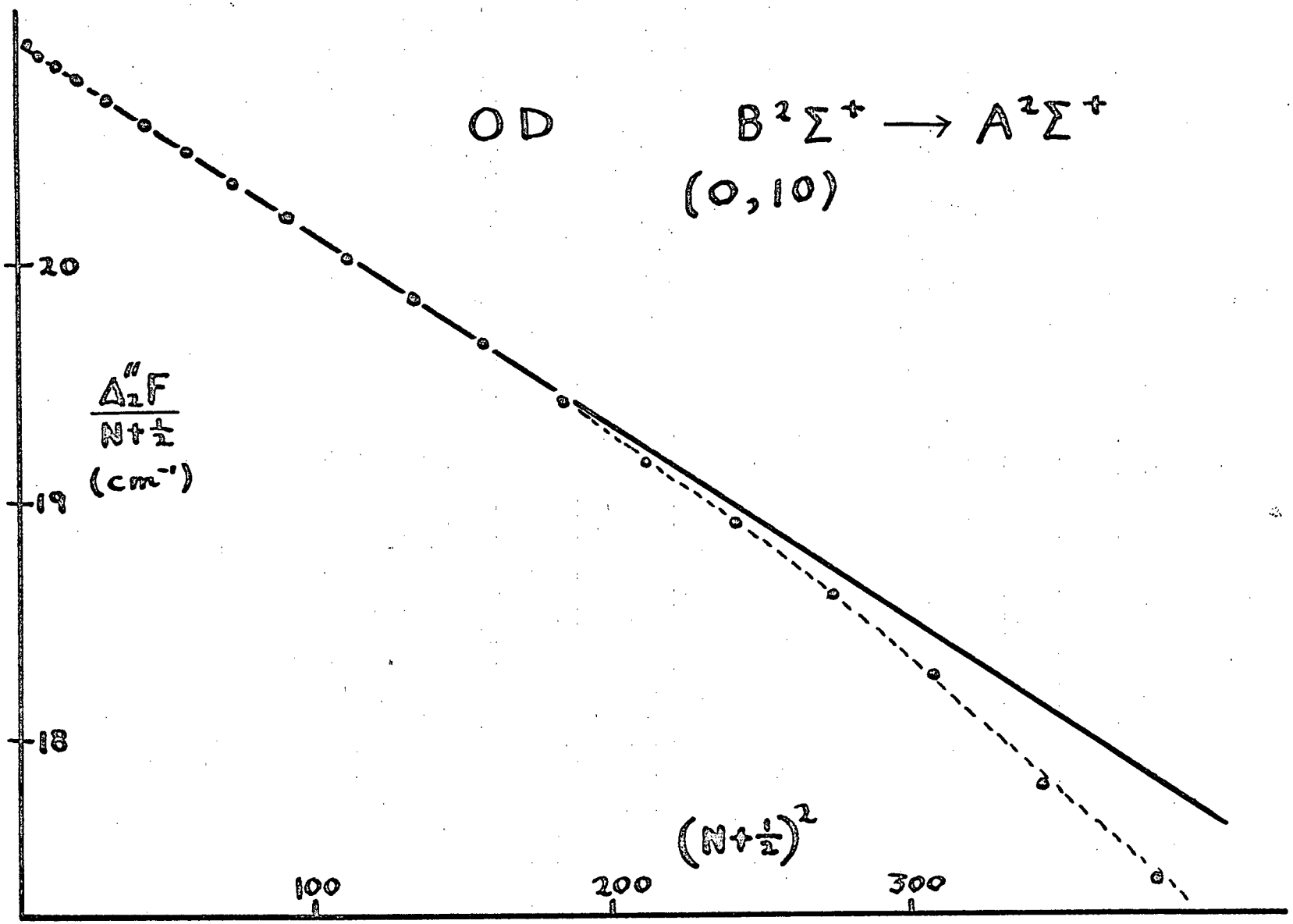

Figure 8. $\frac{\Delta_2'' F}{N+\frac{1}{2}}$ vs $(N+\frac{1}{2})^2$ for v = 10 in the $A^2\Sigma^+$ state of OD.

OH					OD				
State	v	B	D	H	State	v	B	D	H
C	3	a			C	0	2.25		
	2	----							
	1	4.146 [b]	0.2						
	0	4.213	0.2						
$B_e = 4.247$ cm^{-1} ; $\alpha_e = 0.078$ cm .									
$r_e = 2.048$ Å									
$\frac{B_o(OD)}{B_o(OH)} = \frac{2.25}{4.213} = 0.534$; $\rho^2 = 0.529$									
B	1	4.119	2.91	15	B	2	1.947	1.89	
	0	5.086	0.929			1	2.445	0.448	0.16
						0	2.745	0.250	0.12
A	9	5.888	8.63	30	A	13	2.44		
	8	8.342	4.94			12	3.682	4.27	12.2
	7	10.09	3.41			11	4.566	1.33	0.74
	6	11.44	2.65			10	5.239	1.04	0.30
	5	12.53	2.26			9	5.781	0.848	0.22
	4	13.51 [c]	2.00			8	6.276	0.778	
	3	14.222	2.06 [d]			7	6.658	0.613	
	2	15.287	2.06			6	7.046	0.644	
	1	16.129	2.03			3	8.068	0.55	
	0	16.916	2.04			2	8.393	0.55	
						1	8.714	0.54	
						0	9.037	0.55	

Table 11. Rotational constants, in cm^{-1} ; the D values are multiplied by 10^{+3} and the H values by -10^{+6}.

a. Michel's value is 3.96.
b. Michel's value is 4.12.
c. From a study of the $A^2\Sigma^+ \rightarrow X^2\Pi$ system, this value is 13.494.
d. The rotational constants in the $A^2\Sigma^+$ state for v = 0,1,2,3 , in OH and OD, are taken from Barrow (1956)

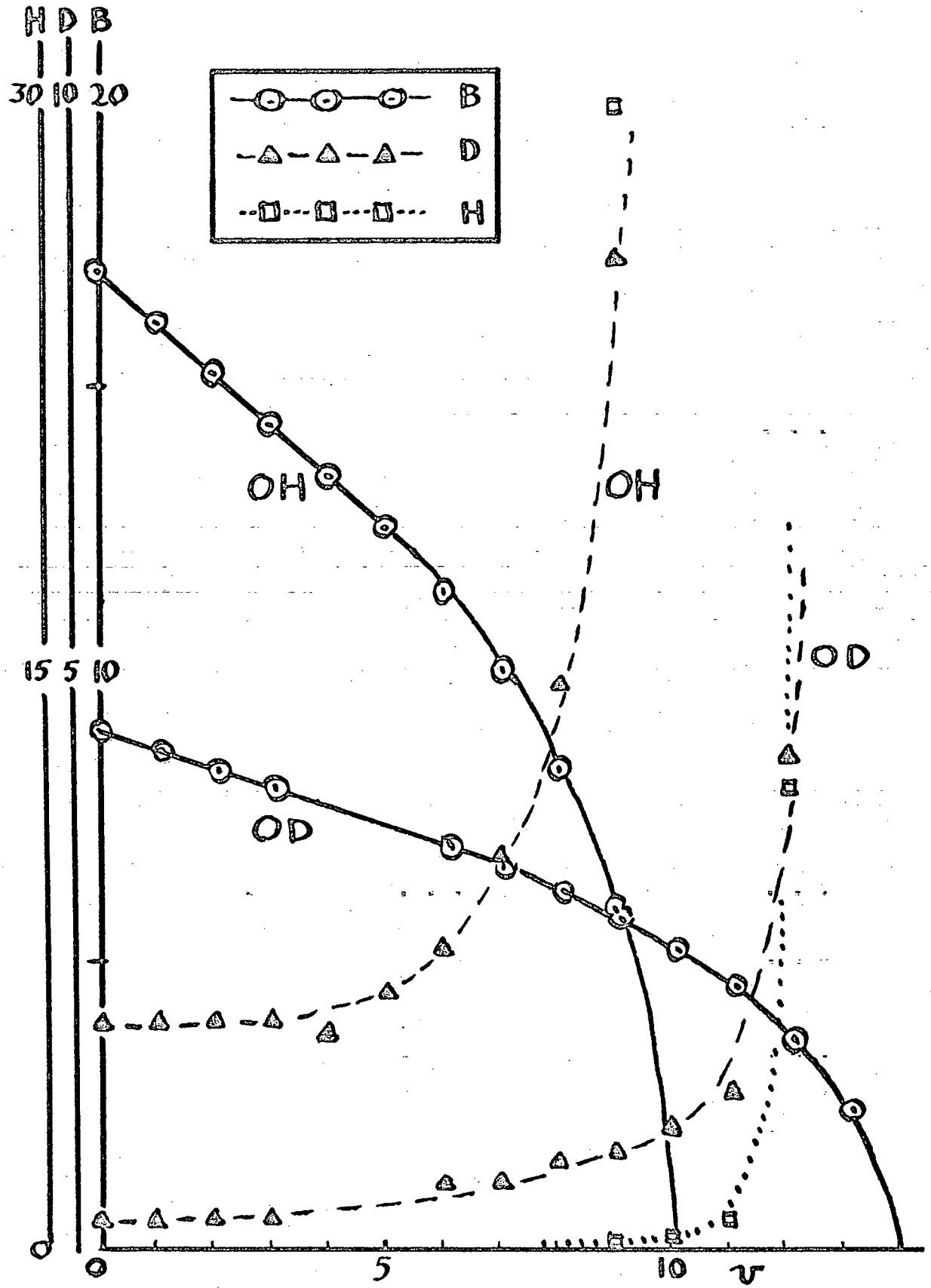

Figure 9. Rotational constants in the $A^2\Sigma^+$ state. The D values are multiplied by 10^{-3} and H by -10^{-6}.

Chapter VII - Dispersion Humps in the $A^2\Sigma^+$ and $B^2\Sigma^+$ States and the Dissociation Energy of OH

(a) Vibrational Quanta of $A^2\Sigma^+$

The vibrational quanta were calculated by taking combination differences between corresponding lines of two bands having the same upper state, that is, (Herzberg, 1950):

(VII - 1): $$R_{v'v_1''}(N) - R_{v'v_2''}(N) = P_{v'v_1''}(N) - P_{v'v_2''}(N)$$
$$= G''(v_2'') - G''(v_1'') - (B_{v_2''} - B_{v_2''})N(N+1) + \cdots$$

Greater accuracy was obtained by adding to the combination differences $(\bar{B}_{v_1''} - \bar{B}_{v_2''})\ N(N+1)$, where $\bar{B}$ indicates the B value as obtained from the combination relations, and plotting the resulting value against $N(N+1)$. A typical plot is shown in Fig. 10, where $\Delta G(8.5)$ is obtained from the $C \rightarrow A$ system. The vibrational quanta are given in tables 12 and 13, together with their experimental values.

(b) Dissociation Energy of $A\ (^2\Sigma^+)$.

In Fig. 11, the experimental values $\Delta G(v + \frac{1}{2})$ for the $A(^2\Sigma^+)$ state of OH and OD are plotted against v. $\Delta G(v + \frac{1}{2}) = G(v+1) - G(v)$.

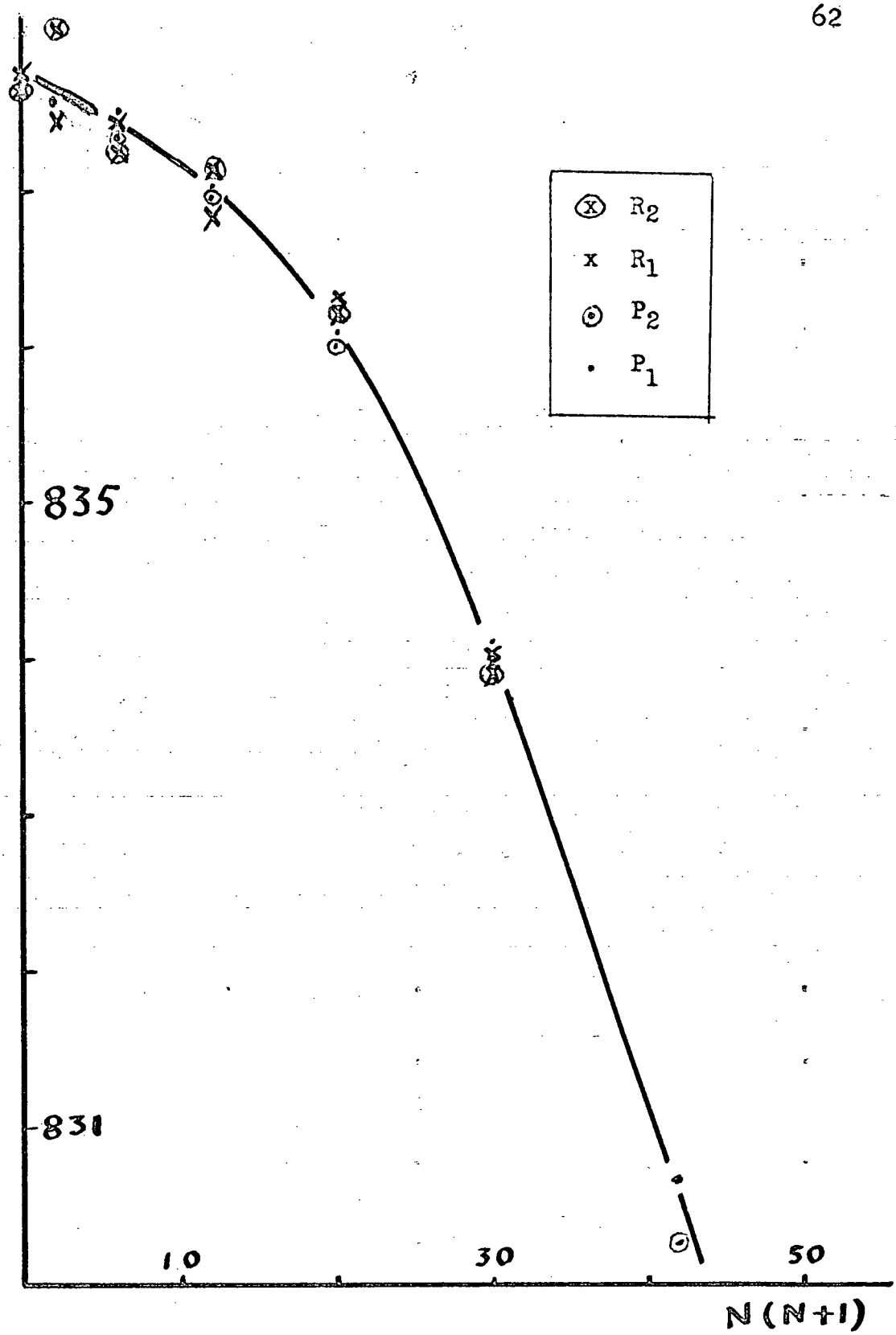

Figure 10. A plot of equation (VII-1) for the (1,9) and (1,8) bands of the C → A system, thus giving $\Delta G(8.5)$ of the $A^2\Sigma^+$ state.

v	$\Delta G(v+\frac{1}{2})$ experimental	ΔG(experimental) - ΔG(calculated) M		
		4[c]	5[d]	6[e]
0	2988.6[a]	0.1	0.1	0.1
1	2793.0[a]	-0.2	-0.3	-0.1
2	2593.5[a]	0.3	0.4	00.1
3	2385.5[a]	0.0	0.1	0.1
4	2162.4 ± 0.4	-0.7	0.3	-0.5
5	1915.6 ± 0.3	0.8	-0.7	-0.3
6	1624.8 ± 0.2	-0.1	-0.2	-0.5
7	1273.8 ± 0.2	-0.1	0.0	0.2
8	837.6 ± 0.2	0.1	0.0	0.0
9		287.7[b]	288.8[b]	297.9[b]
		9.9422	9.9454	9.9773 v-intercept
		18843	18844	18854 D° (cm^{-1})

Table 12. $D^\circ(A\,^3\Sigma^+)$ for OH.

a. Taken from Barrow (1956)
b. Calculated ΔG.

i \ C_i	c	d	e
0	3084.08	3083.71	3086.28
1	-189.316	-188.311	-196.559
2	-4.07043	-4.79355	3.06261
3	0.941340	1.14894	-2.09695
4	-0.176504	-0.202176	0.451410
5		0.C0114100	-0.0619602
6			0.00233708

v	$\Delta G(v+\frac{1}{2})$ experimental	ΔG(experimental)-ΔG(calculated) M		
		4[c]	5[d]	6[e]
0	2214.6[a]	0.1	0.1	0.0
1	2111.5[a]	-0.3	-0.3	0.0
2	2007.5[a]	0.2	00.2	0.0
3		1900.9	1901.0	1901.6[b]
4		1791.9	1792.0	1792.6[b]
5		1678.6	1678.7	1678.9[b]
6	1588.3± 0.5	-0.1	-0.1	0.0
7	1427.9± 0.5	0.2	0.2	0.3
8	1281.5± 0.3	-0.7	0.3	-0.7
9	1117.4± 0.3	0.7	0.8	0.6
10	924.8± 0.2	-0.1	-0.1	-0.2
11	699.8± 0.3	-0.2	-0.2	0.0
12	433.9± 0.5	0.1	0.1	0.0
13		117.7	117.3	120.4[b]
		13.832	13.831	13.845 v-intercept
		19260	19260	19264 D° (cm^{-1})

Table 13. $D^\circ(A^2\Sigma^+)$ for OD.

a. Taken from Barrow (1956)
b. Calculated ΔG.

C_i / i	c	d	e
0	2264.88	2265.00	2266.46
1	-99.9520	-100.229	-104.192
2	-1.77224	-1.61107	1.24785
3	0.305897	0.272176	-0.551900
4	-0.0369535	-0.0340381	0.0782818
5		-0.0000890593	-0.00735406
6			0.000179802

Figure 11. $\Delta G(v+\frac{1}{2})$ vs v for the $A^2\Sigma^+$ state of OH and OD. The area under each curve from v = 0 to the v- intercept is $D^\circ(A^2\Sigma^+)$.

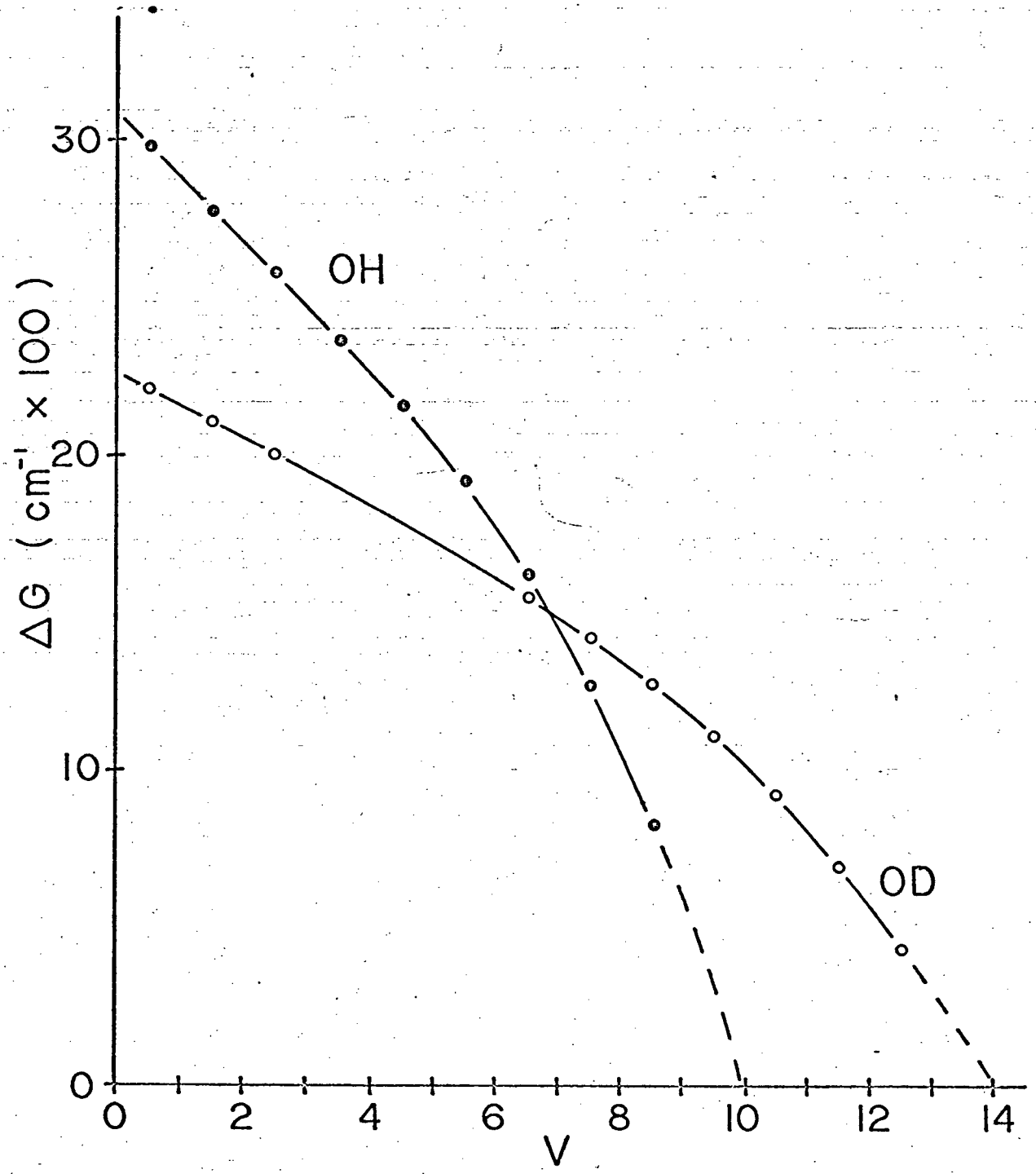

The area under a curve from $v = 0$ to the v - intercept is the dissociation energy D° of that state.* The area was obtained by fitting polynomials

$$\Delta G(v+\tfrac{1}{2}) = \sum_{i=0}^{M} C_i v^i \qquad \text{(VII-2)}$$

and performing the integration. The results of the integration are given in tables 3 and 4 for $M = 4, 5, 6$.+

When the $\Delta G(v + \frac{1}{2})$ were increased by adding to each their experimental values, D° was increased by no more than 3 cm^{-1} in each integration. Similarly, with the $\Delta G(v + \frac{1}{2})$ each decreased by the experimental error, D° decreased by no less than 3 cm^{-1} in each integration. The major error in establishing D° ($A^2\Sigma^+$) arises from the extrapolation of the curves of Fig. 11, beyond the last observed experimental point. The polynomial fitting and the integration were done by computer, and double precision was used to remove round-off errors. All the D° ($A^2\Sigma^+$) values in tables 3 and 4 converge to a value with a spread of $\pm$ 7 cm^{-1} in OH and

---

* A detailed calculation is given in part (d), where the same calculation for 3 points is done by hand and checked by computer.

\+ It was found that with $M < 4$, equation (2) gave poor reproduction of the experimental ΔG . With $M > 6$, the least squares deviation did not change significantly and the calculated ΔG curve behaved peculiarly at low v's.

$\pm$ 3 cm^{-1} in OD. Moreover, the values of the dissociation energy $D^\circ (X\,^2\Pi_{3/2})$ for OH as obtained from the OH data and OD data are in excellent agreement (following section). Assuming that the potential curve of the $A^2\Sigma^+$ state behaves "normally" beyond the last observed vibrational level, the accuracy of the extrapolation of the OH curve is 10 cm^{-1} or better, and of the OD curve it is 5 cm^{-1} or better. We judge a conservative error on $D^\circ (A^2\Sigma^+)$ of OH to be $\pm$ 15 cm^{-1}.

(c) Energy levels in OH and OD

To facilitate discussion, the energy of the vibrational levels in OH and OD are given in table 14. The $J = 1\frac{1}{2}$ level of $v = 0$ of $X\ (^2\Pi_{3/2})$ of OH is taken as 0.0 (all units in cm^{-1}). The $P_1(1)$ transition of the $A \rightarrow X$ system of OH is 32440.6 (Dieke and Crosswhite, 1948). The dissociation limit of $A^2\Sigma^+$ of OH is then 51287.6 ± 15, from table 14. Taking the dissociation limit of $A^2\Sigma^+$ of OH and OD to be coincident, from table 14, the $v = 0$ level of $A^2\Sigma^+$ of OD is 32024.6. The $P_1(1)$ transition of the $A \rightarrow X$ system of OD is 32528.5 (Ishaq, 1937) and the $J = 1\frac{1}{2}$ level of $v = 0$ of $X\ ^2\Pi_{3/2}$ of OD is -503.9.

The difference in energy of the $v = 0$ levels of OH and OD in the $X\ (^2\Pi_{3/2})$ state comes from the different vibrational frequencies of the two molecules and from the zero point correction (Dunham, 1932). The total difference is calculated to be 498.1 (Appendix III). This is in excellent agreement with the experimental value (503.9 ± 15). The minima of the potential curves of OH and OD are not expected to coincide because of electronic isotope shifts. Bunker (1968) calculates these shifts to be of the order of $5 \sim 10$ cm^{-1}. *

---

* Appendix VI treats electronic isotope shifts in greater detail.

	OH		OD	
State	v	Energy	v	Energy
$X^2\Pi_{3/2}$	0	0.0	0	-503.9
	Calculated dissociation limit			35419.9
$A^2\Sigma^+$	0	32440.6	0	32024.6
	1	35429.2	1	34239.2
	2	38222.2	2	36350.7
	3	40815.7	3	38358.2
	4	43201.2	4	40259.4
	5	45363.6	5	42051.6
	6	47279.2	6	43730.4
	7	48904.0	7	45288.7
	8	50177.8	8	46716.6
	9	51015.4	9	47998.1
			10	49115.5
			11	50040.3
			12	50740.1
			13	51174.0
	Calculated dissociation limit			51287.6 ± 15
$B^2\Sigma^+$	0	68406.1	0	68300.3
	1	69065.8	1	68847.2
			2	69205.1
	Calculated dissociation limit			69212.3
$C^2\Sigma^+$	0	88261.3	0	88114.9
	1	89456.0		
	2	---		
	3	91731.0		
	Calculated dissociation limit			117679

Table 14. Energy values (cm^{-1}) of the vibrational levels. The dissociation limit of the A state is calculated from the ΔG's of that state. The dissociation limit of the X, B, C, states is deduced from atomic data.

The energy separations O (^1D) - O ($^3P_2$) and O (^1S) - O (^1D) are well known (Moore, 1952). (Fig. 12) The calculated dissociation limit of O (^1S) + H (^2S), i.e. OH ($B^2\Sigma^+$), is 69212.3 $\pm$ 15 and that of O ($^3P_2$) + H (^2S) is 35419.9 $\pm$ 15. The dissociation limit D° of the hydroxyl radical is the difference between J = 1.5 in v = 0 of X $^2\Pi_{3/2}$ and the dissociation limit O ($^3P_2$) + H (^2S) which is (35419.9 $\pm$ 15) cm^{-1}.+

+ A slightly better value could be obtained if the electronic isotope shift in the ground state were known. D° ($A^2\Sigma^+$) of OD could then be used exclusively.

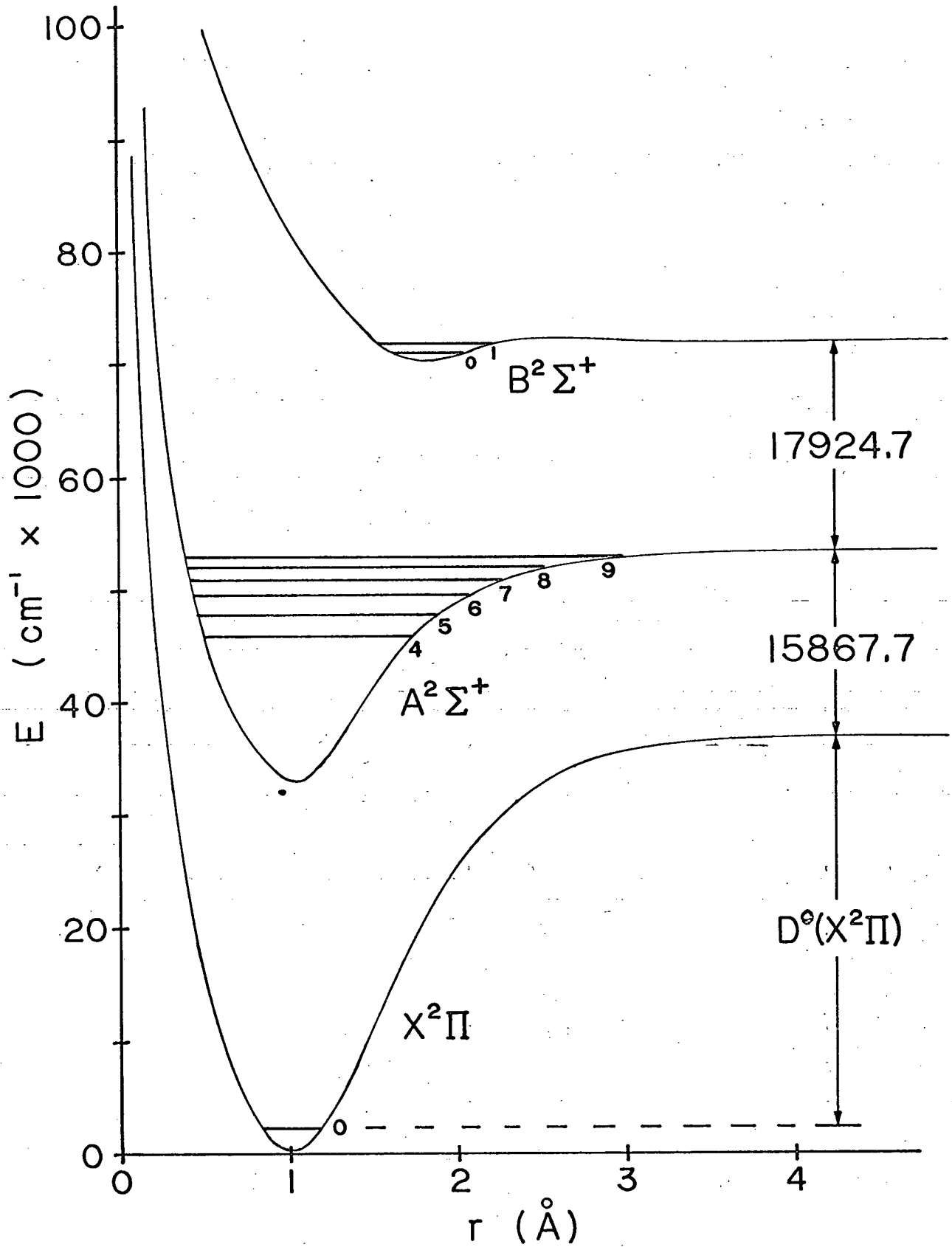

Figure 12. Atomic data used to calculate $D^{\circ}(X^{2}\Pi)$. The vibrational levels observed in OH are also shown.

(d) Dissociation Energy of $B^2\Sigma^+$ State

For the B state, the experimental vibrational quanta are, for OH, $\Delta G(0.5) = 659.7\ cm^{-1}$ and for OD, $\Delta G(0.5) = 546.9\ cm^{-1}$ and $\Delta G(1.5) = 357.9\ cm^{-1}$. For a three term expantion of the vibrational energy, that is

$$G(v) = \omega_e(v+\tfrac{1}{2}) - \omega_e x_e(v+\tfrac{1}{2})^2 + \omega_e y_e(v+\tfrac{1}{2})^3$$

then

$$G(v+1) - G(v) = \omega_e - \omega_e x_e(2v+2) + \omega_e y_e(3v^2+6v+13/4)$$

Using the isotopic relations, one must solve

$$\begin{aligned} 659.7 &= \omega_e - 2\omega_e x_e + 3.25\,\omega_e y_e \\ 546.9 &= \rho\omega_e - 2\rho^2\omega_e x_e + 3.25\,\rho^3\omega_e y_e \\ 357.9 &= \rho\omega_e - 4\rho^2\omega_e x_e + 12.25\,\rho^3\omega_e y_e \end{aligned}$$

The solution is

$$\begin{aligned} \omega_e &= 976.5\ cm^{-1} \\ \omega_e x_e &= 109.3\ cm^{-1} \\ \omega_e y_e &= -20.99\ cm^{-1} \end{aligned}$$

Also,

$$\begin{aligned} \Delta G^{OD}(2.5) &= 119.7\ cm^{-1} \\ \Delta G^{OH}(1.5) &= 252.2\ cm^{-1} \end{aligned}$$

To find the v intercept of the $\Delta G(v)$ curve, one needs to solve

$$\frac{dG}{dv} = 0 = \omega_e - 2\omega_e x_e(v_0+\tfrac{1}{2}) + 3\omega_e y_e(v_0+\tfrac{1}{2})^3$$

which gives $v_0 = 2.512$.

The dissociation energy D_e of the $B^2\Sigma^+$ state is then

$$D_e = \omega_e(v_0+\tfrac{1}{2}) - \omega_e x_e(v_0+\tfrac{1}{2})^2 + \omega_e y_e(v_0+\tfrac{1}{2})^3 = 1355 \text{ cm}^{-1}$$

It is difficult to assess the error, since the $B^2\Sigma^+$ state is very shallow and the isotope relations were invoked.

Predissociation by rotation* has been reported by Felenbok (1963) for the $B^2\Sigma^+$ state of OH, who determined the dissociation energy of the B state to be 1315 cm^{-1}. Felenbok gives convincing evidence that $N = 15$ is the last rotational level of the $v = 0$ state. He did not see the same sudden drop in intensity for the $v = 1$ level and assumed that $N = 8$ is the last rotational level in $v = 1$ as he saw no more levels. We have seen $N = 9$ in $v = 1$ and assuming that this is the last rotational level, the limiting curve of dissociation gives an apparent D_e ($B^2\Sigma^+$) = 1360 cm^{-1}. This value agrees extremely well with that obtained by the ΔG (v) method.

The limiting curve of dissociation has been redrawn in Fig. 13 with the energy measured from the $v = 0$ of the X ($^2\Pi_{3/2}$) state of OH. This procedure has the advantage

---

* Predissociation by rotation is a consequence of the term $\frac{P^2}{2\mu r^2} = \frac{P^2}{2\mu r_e^2}\left(1 + \frac{\xi}{r_e} + \cdots\right)$ in equation (II-2). Herzberg (1950) discusses predissociation by rotation and the limiting curve of dissociation in great detail.

that the error in establishing the $v = 0$ level relative to the minimum of the $B^2\Sigma^+$ state is absent. From Felenbok's data $F(15)$ in $v = 0$ is $1165.2\ cm^{-1}$ and from our data, $F(9)$ in $v = 1$ is $347\ cm^{-1}$. $F(16)$ in $v = 0$ is calculated to be $1312.7\ cm^{-1}$ and $F(10)$ in $v = 1$ is calculated to be $417\ cm^{-1}$.

The dissociation limit of the $B^2\Sigma^+$ state is found from Fig.13 to be $69323\ cm^{-1}$. A lower limit, from Fig.13 is $69265\ cm^{-1}$. For comparison, from table 14, the dissociation limit of the $B^2\Sigma^+$ state is calculated to be $(69212 \pm 15)\ cm^{-1}$, from the ΔG vs v curves of Fig. 11.

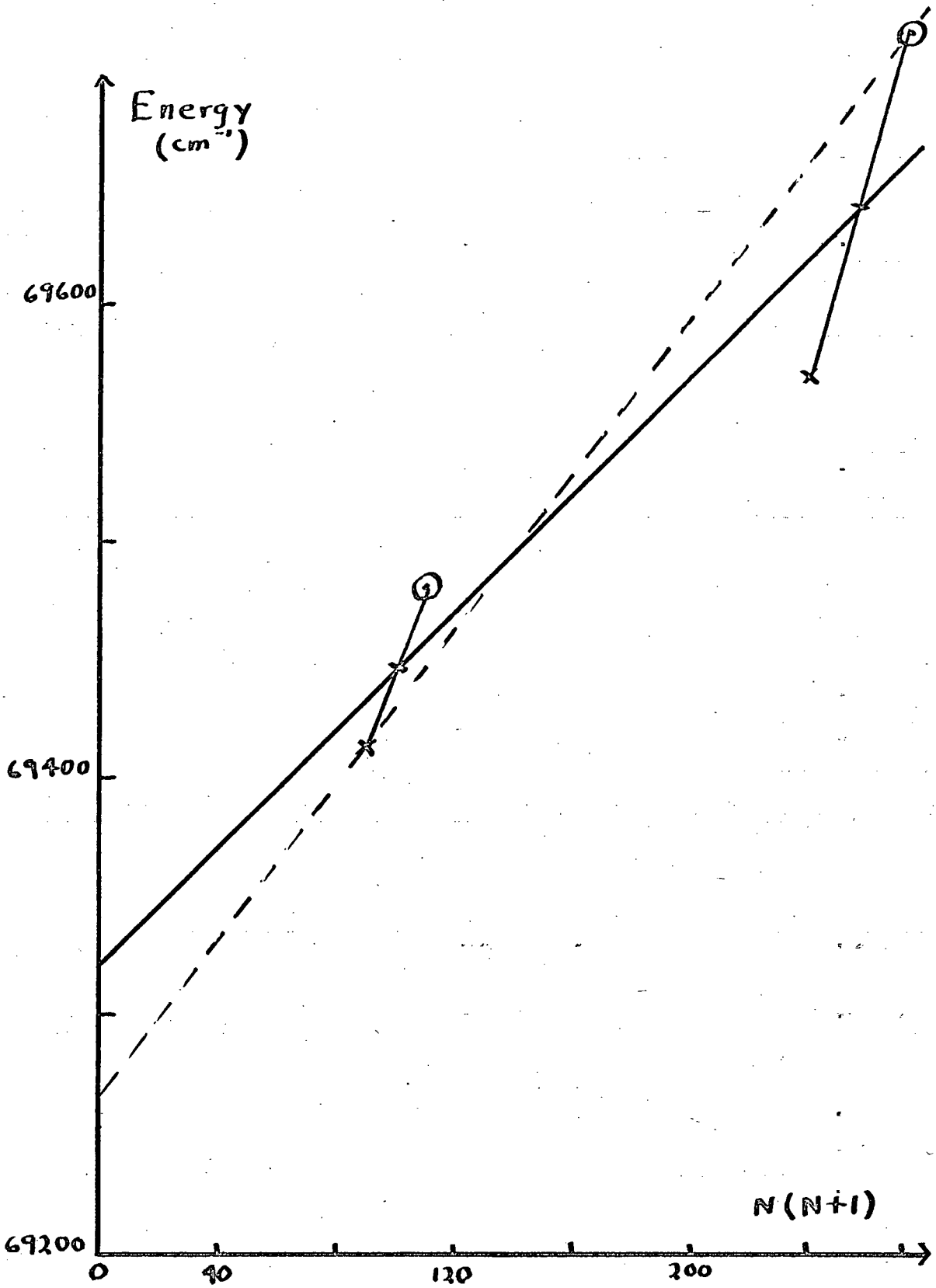

Figure 13. The limiting curve of dissociation for the $B^2\Sigma^+$ state of OH. The energy is measured from v=0 of $X^2\Pi_{3/2}$.

(e) Discussion

The dissociation energies D° ($A^2\Sigma^+$) of OH and OD as calculated from the areas under the curves of Fig. 11 predict the dissociation energy D° ($X\ ^2\Pi_{3/2}$) of OH to be $(35420 \pm 15)\ cm^{-1}$.

The dissociation limit of the $B^2\Sigma^+$ state is similarly deduced to be $(69212 \pm 15)\ cm^{-1}$ above v = 0 in $X\ (^2\Pi_{3/2})$ of OH. Direct calculation of the dissociation limit of $B(^2\Sigma^+)$ is 69323 cm^{-1} and our estimates of error do not reduce this value to the deduced value. That this discrepancy is not due to errors can further be seen from table 14, where v = 2 in the $B^2\Sigma^+$ state of OD is extremely close to the deduced dissociation limit of the $B(^2\Sigma^+)$ state and we have seen N = 9 in this v = 2 level, which lies 159 cm^{-1} above N = 0. Either the extrapolation of the curves of Fig. 11 does not follow the dashed portions, or dispersion humps are causing the discrepancy. Since v = 13 in $A\ (^2\Sigma^+)$ state of OD is only 114 cm^{-1} from the expected dissociation limit of $A\ (^2\Sigma^+)$ and v = 9 in OH is 272 cm^{-1} from the same limit, and D° ($A^2\Sigma^+$) of OH and OD both predict D° ($X\ ^2\Pi_{3/2}$) of OH to such a good agreement, we cannot believe the first

alternative. It is quite possible that the dispersion hump in the B ($^2\Sigma^+$) state is about 100 cm^{-1} larger than that in the A ($^2\Sigma^+$) state. *

We have no way of knowing how large the hump in the A ($^2\Sigma^+$) state is. Assuming that the dissociation energy of the A state is given correctly by the area under the ΔG curves of Fig. 11, an upper bound to the dissociation energy of the ground state of OH is (35420 $\pm$ 15) cm^{-1}. The true dissociation energy is less by an amount equal to the height of the dispersion hump of the A ($^2\Sigma^+$) state.

The slope of the limiting curve of dissociation predicts the maximum value of the hump in the $B^2\Sigma^+$ of OH state at an internuclear distance of 3.8 Å.

---

* Kolos and Wolniewicz (1965) have calculated a dispersion hump of height 105 cm^{-1} at r = 4.75 Å in the $^1\Pi_g$ state of H_2.

Chapter VIII - Vibrational constants of $C(^2\Sigma^+)$ and $B(^2\Sigma^+)$

In the investigation of the C state, a vibrational level was found below the one labelled v = 0 by Michel (1957). In this section, proof is given through the isotopic relations that the v numbering in the C state as given here, is correct and that Michel actually observed that (1,8), (1,7), (1,6), (3,7) and (3,6) transitions of the $C \rightarrow A$ system of OH.

(a) Vibrational Constants of the C state.

The measured $\Delta G(0.5)$ of OH is 1194.7 cm^{-1}. Michel measured $\Delta G(1.5) + \Delta G(2.5) = 2275$ cm^{-1}. With these values, $\omega_e = 1232.9$ cm^{-1} and $\omega_e x_e = 19.1$ cm^{-1}. Using the isotopic relations it is straight forward to calculate G(0) both for OH and OD and the Dunham zero point corrections, (Appendix III). Since the v = 0 energy are known, table 14, it is found that the energy of the minimum of the potential is (87650 $\pm$ 15) cm^{-1} for OH and (87668 $\pm$ 15) cm^{-1} for OD. The agreement is quite good. *

---

* Because of electronic isotopic shifts, the two minima are not expected to have the same energy.

The next $^2\Sigma^+$ state allowed by the Wigner-Witmer rules beyond the $B^2\Sigma^+$ state is $O(^3P) + H(^2P)$, arising from the configuration $O(1s^2 2s^2 2p^4) + H(2p)$. The dissociation limit of this state lies 82259 cm^{-1} above the dissociation limit of the ground state of OH (Moore, 1952). Since terms of like species cannot cross and taking the dissociation energy of the ground state given in Chapter VII, $D^\circ (C^2\Sigma^+) = (29418 \pm 15)$ cm^{-1}.

T_e for the $C^2\Sigma^+$ state of OH is obtained by adding to 87650 cm^{-1}, G(0) and Yoo of the ground state. T_e = (89500) cm^{-1}.

The electronic energy level of OH including the C state is given in Fig. 14. The identification of the C state with atomic states has always been debated (Barrow, 1956), Michel (1957). There is now no doubt about the T_e value of the C state. Some $^2\Sigma^+$ states allowed by the Wigner-Witmer rules beyond $B^2\Sigma^+$ are $O(^3P) + H(^2P)$ arising from the $O(1s^2 2s^2 2p^4) + H(2p)$, $O(^1D) + H(^2S)$ arising from $O(1s^2 2s^2 2p^4) + H(2s)$, $O(^1D) + H(^2P)$ from $O(1s^2 2s^2 2p^4) + H(2p)$, $O(^1S) + H(^2S)$ from $O(1s^2 2s^2 2p^4) + H(2s)$, and possibly $O^- + H^+$ or $O^+ + H^-$. The energy of these states above v = 0 of X ($^2\Pi_{3/2}$) of OH is 117678 $\pm$ 15, 133546 $\pm$ 15,

133546 $\pm$ 15, 133227 $\pm$ 15, 133267 $\pm$ 40 and 138984 $\pm$ 160 cm^{-1} respectively. The election affinity of oxygen is (1.465 $\pm$ 0.005) ev (Branscomb et al. 1958) and that of Hydrogen is (0.77 $\pm$ 0.02) ev (Weisner and Armstrong, 1964).

Michel correlated the C state with $O^- + H^+$. This may be so, but because of the non-crossing rule, the dissociation limit of the C state is $O\,(^3P) + H(^2P)$.

It is interesting to note that $\Delta G\,(v + \frac{1}{2})$ vs v curve for the C state has positive curvature, rather than the usual negative curvature of Fig. 11. The dissociation limit of the C state by linear extrapolation is

$$D^e = \frac{\omega_e^2}{4\omega_e x_e} = 19900 \text{ cm}^{-1},$$

but D^o has already been given as (29418 $\pm$ 15) cm^{-1}.

(b) Vibrational Constants of the B state.

The B state is very shallow, in fact only two levels have been seen in OH and 3 in OD. With the help of the isotopic relations and using all the observed vibrational quanta of the B state, it has been found in Chapter VII - (d), that

$$\omega_e = 946.5$$
$$\omega_e x_e = 109.3 \text{ cm}^{-1}$$
$$\omega_e y_e = -20.99 \text{ cm}^{-1}$$

Although these constants reproduce the observed $\Delta G\ (v + \frac{1}{2})$ exactly, they predict, for example, $\Delta G(1.5)$ for OH to be 272.2 cm^{-1}. The energy of the $v = 2$ level of OH would be 69318 cm^{-1}, which very likely does not exist (table 14). In view of this awkward situation, the meaning of the vibrational constants of the C state is not very clear.

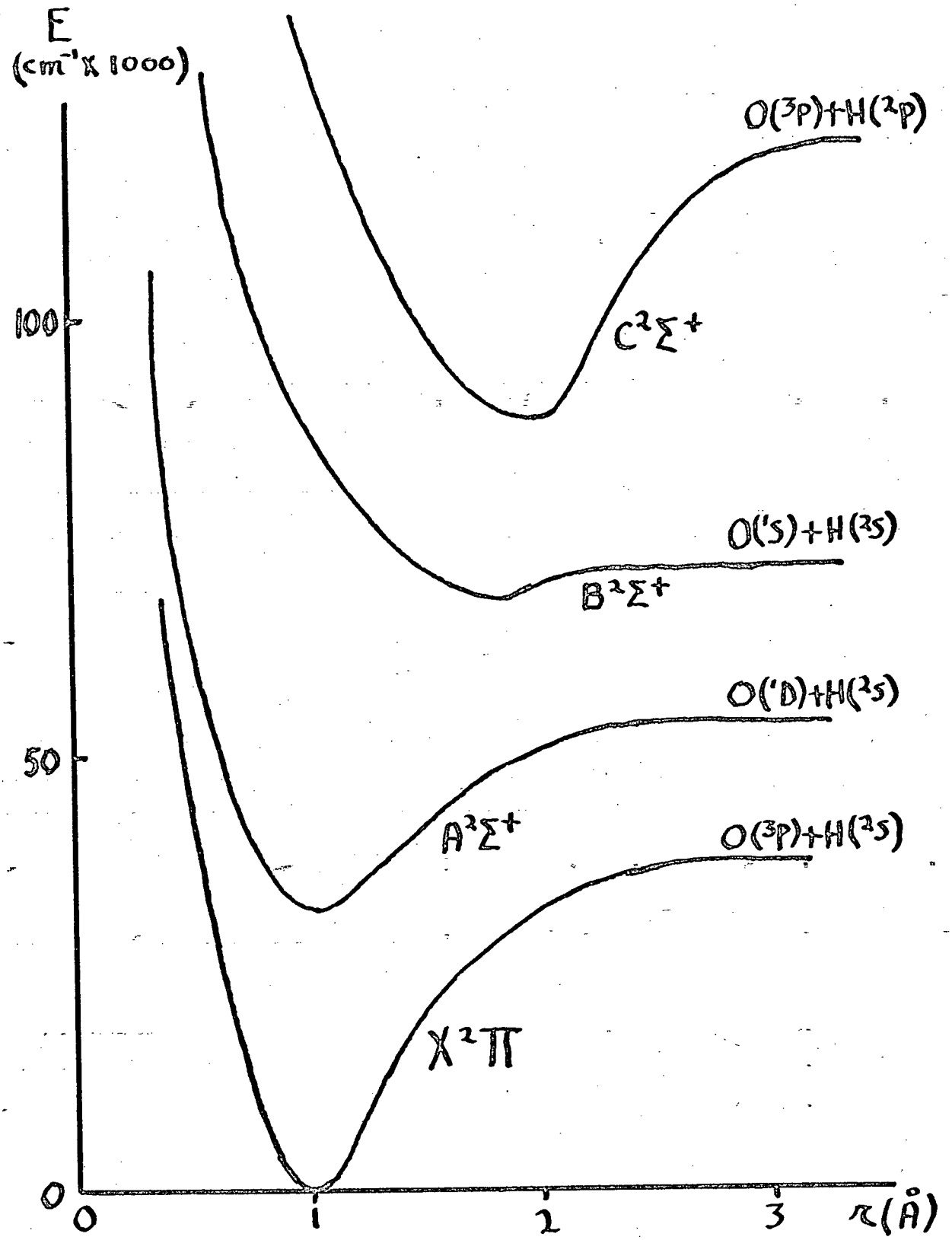

Figure 14. Observed bound states of the hydroxyl radical.

Chapter IX - A Strong Predissociation in the $A^2\Sigma^+$ State of OH

(a) Gaydon Predissociation

A weak predissociation in the $A^2\Sigma^+$ state of OH was first detected by Gaydon and Wolfhard (1951). These investigators found that in the $A \rightarrow X$ system, the intensity of the transitions originating in the $v = 1$ level of $A^2\Sigma^+$ become abnormally weak beginning at $J' = 22\frac{1}{2}$. They found the same weakening of intensity for all the levels in $v = 2$. Charton and Gaydon (1958) have later found that the $v = 3$ levels is also affected by the weak predissociation. Naegeli and Palmer (1967) have found that all the levels beyond $J = 29\frac{1}{2}$ in the $v = 0$ level are affected by the predissociation too. Naegeli and Palmer (1968) have also studied the predissociation in OD. This predissociation at low v's, henceforth referred to as "weak predissociation" or "Gaydon predissociation" is characterized by the fact that the levels with $J = N + \frac{1}{2}$ are affected more than those with $J = N - \frac{1}{2}$. To explain this fact Gaydon proposed the theory that a slightly attractive $^2\Sigma^-$ state is responsible for the predissociation. This theory is shown in Figure 15. Because of the strict

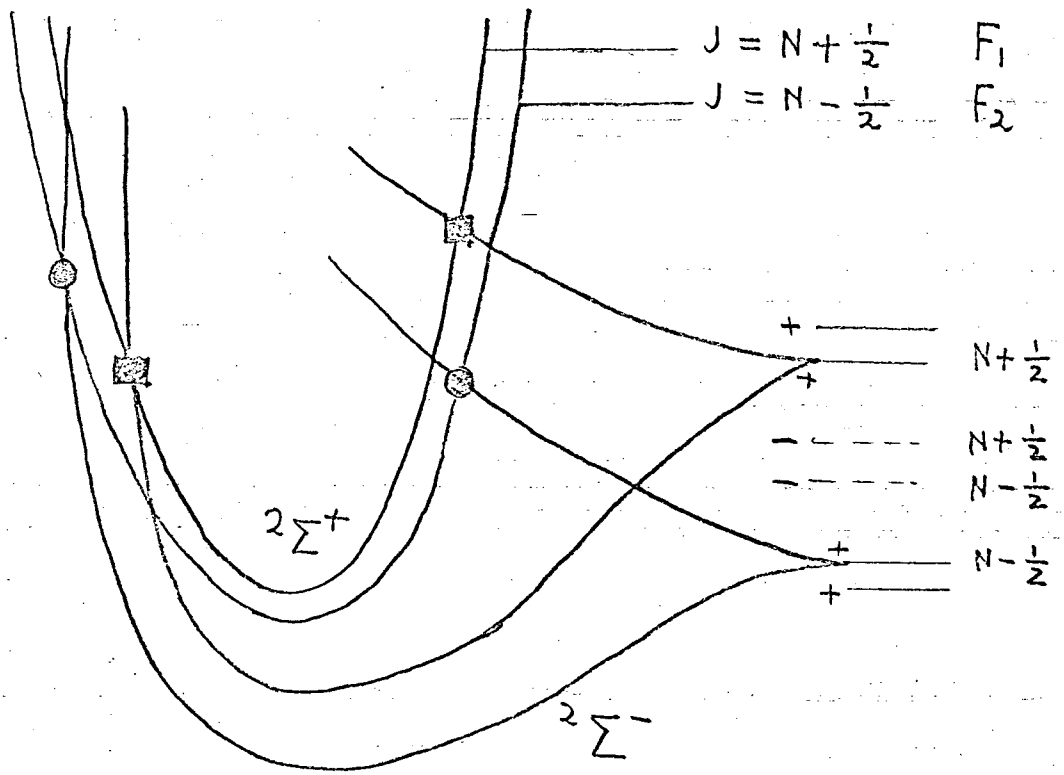

Figure 15. Gaydon Predissociation

selection rules $\Delta J = 0$ and the parity must be same, the only way that the F_1 level can be predissociated more than the F_2 level is that the $^2\Sigma^-$ is repulsive.

The lifetime of the $v = 0$ level of $A^2\Sigma^+$ of OH is 0.99×10^{-6} seconds (Bennett and Dalby, 1964). Since the Gaydon predissociation in the $A^2\Sigma^+$ state was detected through small intensity changes, the lifetime of the $v = 1,2,3$ levels cannot be too much different from 10^{-6} seconds. The Gaydon predissociation is thus weak.

In summary, the characteristics of the Gaydon predissociation are the following:

(1) it sets in near $v = 2$ in OH

(2) one of the spin components is effected more than the other

(3) it is weak

(b) Strong Predissociation

Regarding the predissociation at high v's reported in this work, it was detected through broadening of the rotational transitions. The "average" full width at half maximum is $0.6\ cm^{-1}$. From the Heisenberg relation

$$\Delta E \cdot \Delta t \approx \hbar$$

the average lifetime of the predissociated levels is $\approx 10^{-11}$ seconds. The predissociation at high v's is thus strong.

Plate III shows the (0,8) and (0,7) transitions of the $B \rightarrow A$ system of OH. Since these transitions begin in the same upper state, the predissociation occurs in the lower state. The line broadening cannot be due to thermal broadening, Stark broadening, nor collissional broadening because some of the OH lines appear sharp and others do not.

The molecular H_2 lines identified also appeared sharp. The broadening due to these effects is calculated in Appendix V.

It was found that the variation in half-width is very different from band to band. In the (0,8) and (0,11) bands of OD, the transitions begin broad, but become very sharp at high N. The very opposite is true in the (0,9) band. In (0,10), the transitions are broad at first, then sharp, and then broad again. These results are summarized in Fig. 17 and 18. In each of these Figures, the black dots refers to an unresolved P transitions, the circles to R transitions. The large dots refer to spin unresolved components, the small dots to spin-resolved components. The dotted lines were obtained by subtracting the calculated spin splitting from the unresolved transitions.

In contrast to the Gaydon predissociation, both spin components are equally affected, within our experimental error.

The maximum half-width of the rotational levels within a vibrational state is plotted in Fig. 19. The strong predissociation becomes detectable between v = 6 and 7 in OD, which is about 13,500 cm^{-1} above the minimum of the $A^2\Sigma^+$ state. Fig. 19 should be taken for its qualitative features

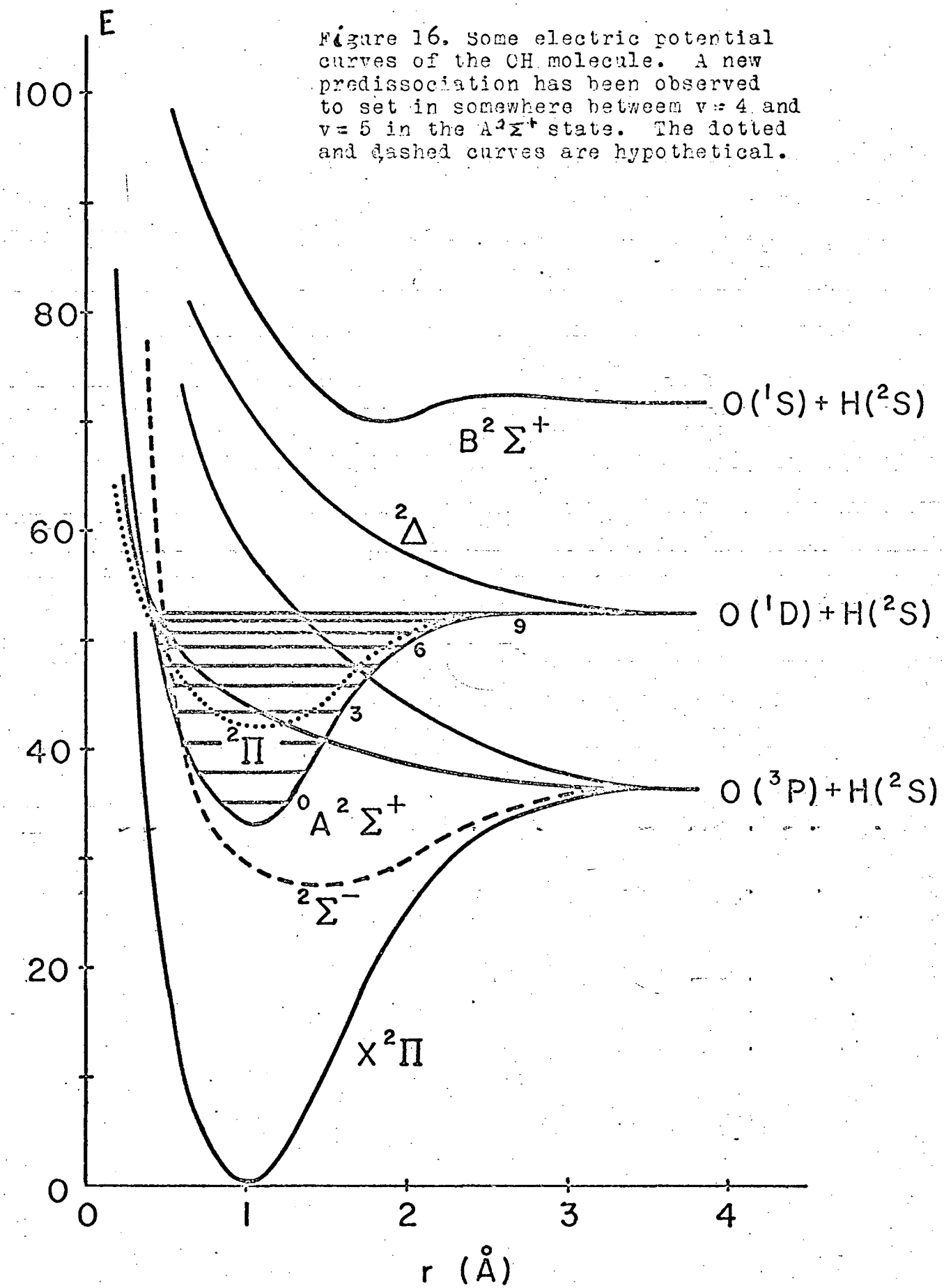

Figure 16. Some electric potential curves of the CH molecule. A new predissociation has been observed to set in somewhere between v = 4 and v = 5 in the $A^2\Sigma^+$ state. The dotted and dashed curves are hypothetical.

Figure 17. Variation of the full width at half maximum of the rotational levels of v = 10 of $A^2\Sigma^+$ in OD. The linear extrapolation at low N values was obtained by subtracting the calculated spin doubling from the unresolved P and R transitions.

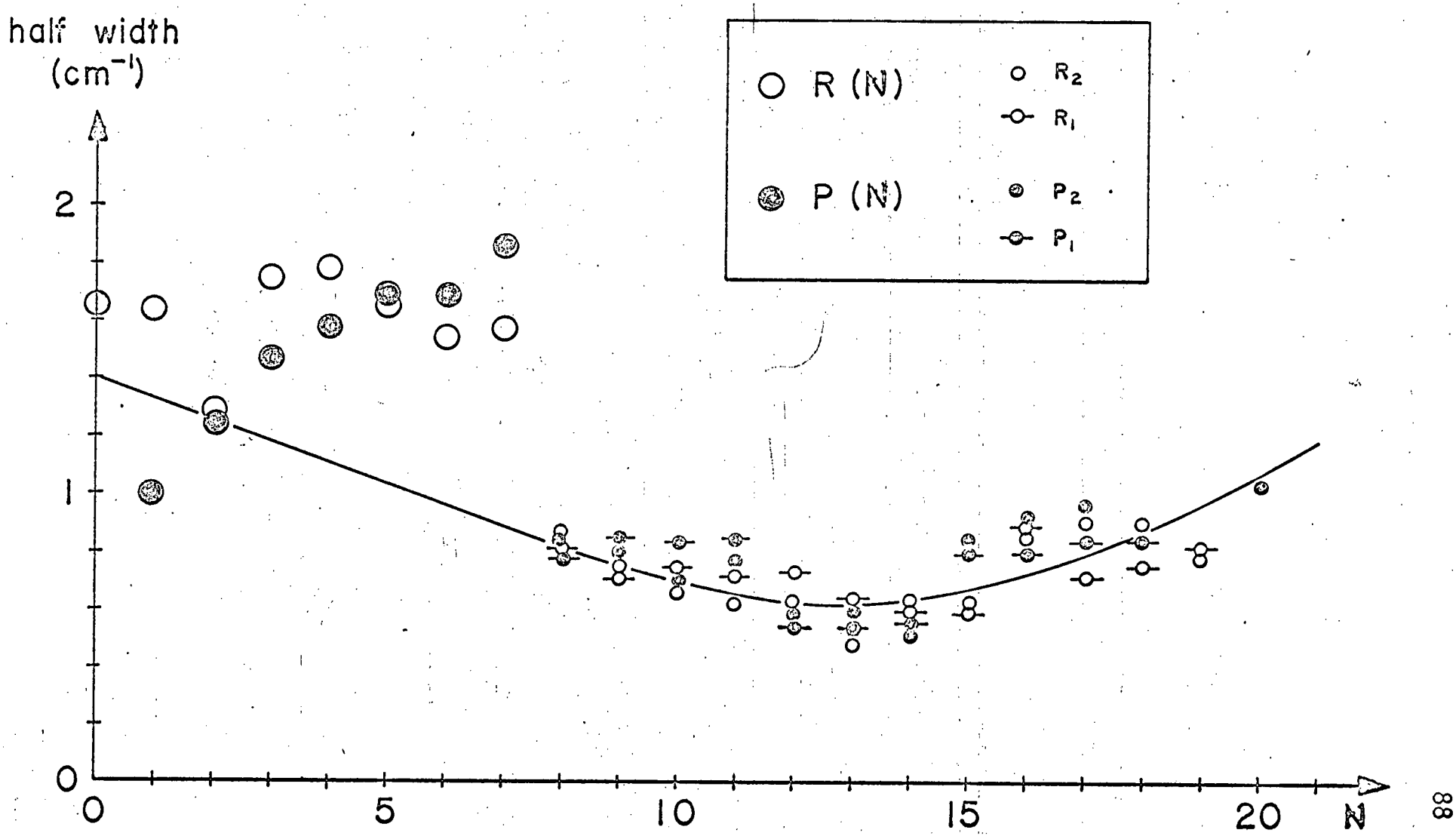

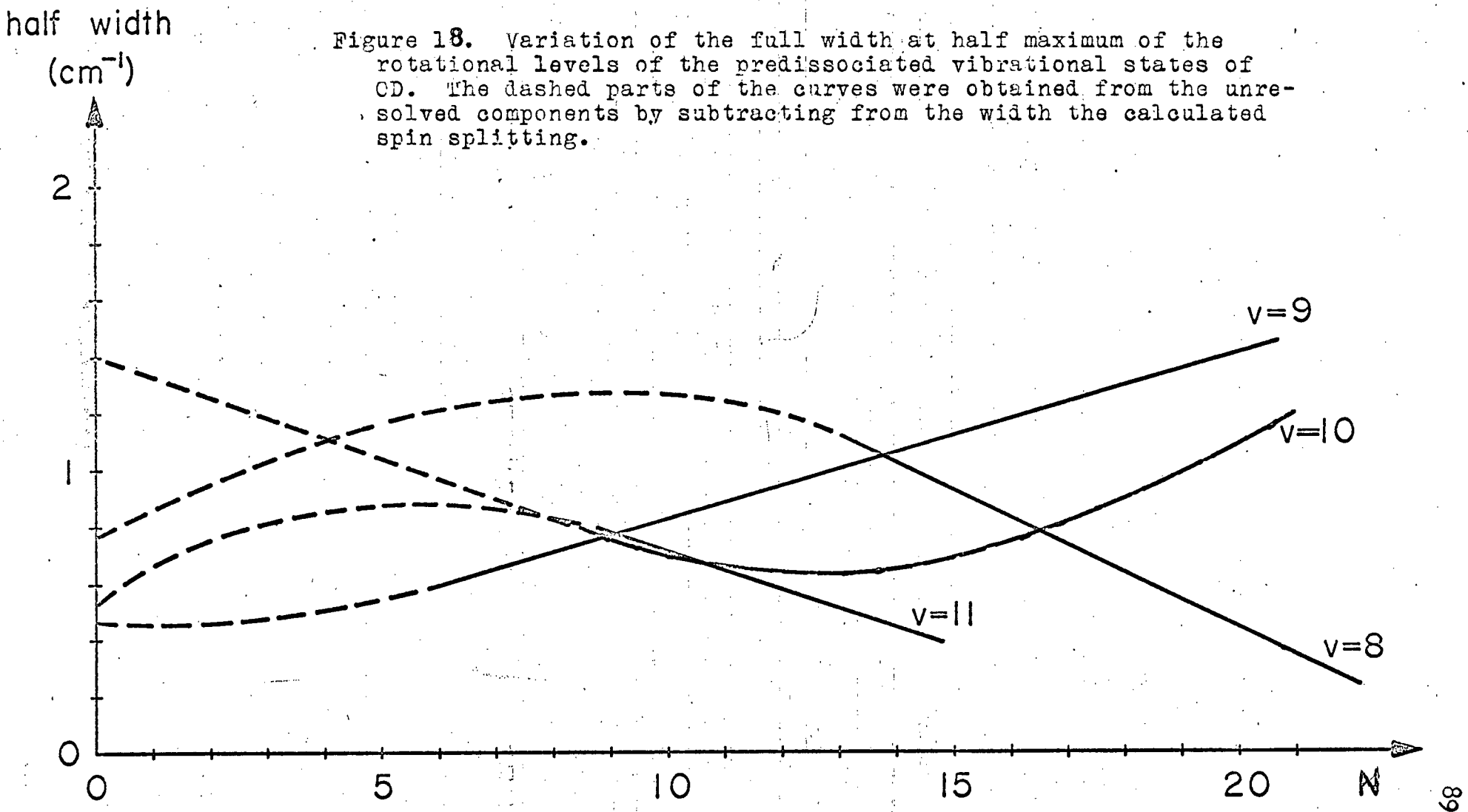

Figure 18. Variation of the full width at half maximum of the rotational levels of the predissociated vibrational states of CD. The dashed parts of the curves were obtained from the unresolved components by subtracting from the width the calculated spin splitting.

Figure 19. The maximum full width at half maximum of the rotational levels within a band. The predissociation sets in at about 13500 cm^{-1} above the miminum of the $A^2\Sigma^+$ state. Czarny and Felenbok (1968) have observed that v = 8 in OH is also predissociated.

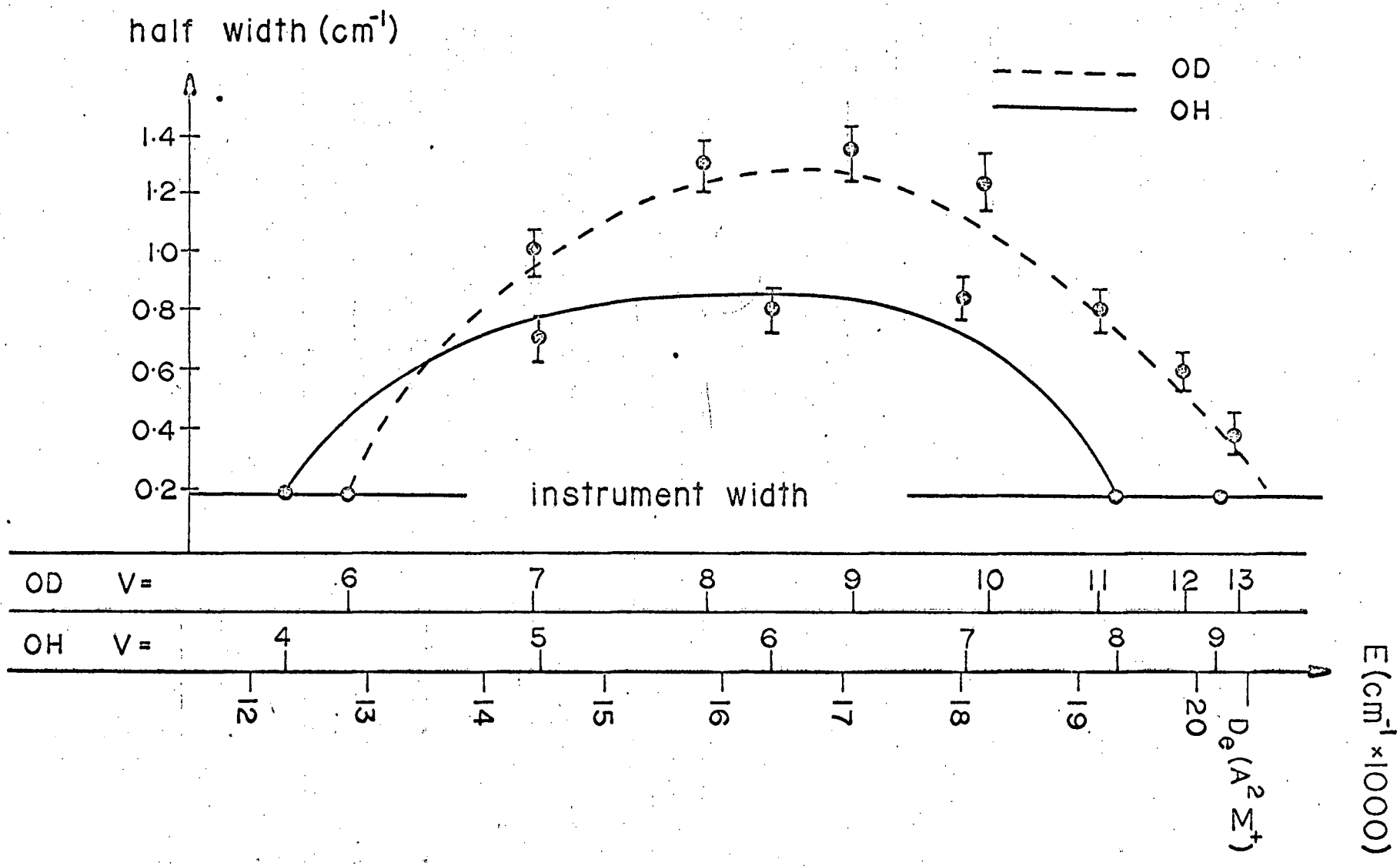

only. Since the data for OD bands comes for 20 transitions in each band and that of OH from 7 transitions only, and since the half breadth is strongly dependent on N, the two curves would probably look more alike if more transitions had been seen in OH.

The observed facts regarding the strong predissociation can be summarized as follows:

(1) it is strong

(2) it becomes detectable between v = 6 and 7 in OD

(3) the predissociation shows definite dependence on the rotation

(4) within the accuracy of the experimental error, both spin components are equally broad.

(c) Reconciliation with theory

Present theory pertaining to predissociations can be summarized as follows

(1) According to the Wigner-Witmer rules when O (^{3}P) and H (^{2}S) combine, the resulting states are $X\,^2\Pi$, $^4\Pi$, $^4\Sigma^-$, $^2\Sigma^-$.

(2) On the basis of selection rules for predissociation, interaction between $A^2\Sigma^+$ and either of $^4\Pi$, $^2\Sigma^-$, $^4\Sigma^-$ leads to weak effect.

(3) Kovacs (1958) has calculated matrix elements for perturbations. Between $^2\Sigma^+$ states and $^2\Sigma^-$, $^4\Sigma^-$, $^4\Pi$ his calculations show no J dependence.

(4) The extent of predissociation depends on the overlap between the wave functions of the repulsive state and the bound state. The overlap is very sensitive to the vibrational state and to the effect of rotation.

In applying these results, none of the $^4\Pi$, $^4\Sigma^-$, $^2\Sigma^-$ can account for the strong predissociation observed at high v's.

Interaction between $^2\Sigma^+$ and $^2\Pi$ leads to strong effects. If the $^2\Pi$ comes from O (^{1}D) + H (^{2}S), perhaps it is bound as shown in Fig. 16. Predissociation then occurs in two steps, first to the $^2\Pi$ and then to the $^2\Sigma^-$. It is also possible that the X $^2\Pi$ ground state comes sufficiently close to the A state near v = 5 at high v's that predissociation takes place through the X $^2\Pi$ ground state. Fig. 17 and 18 show that the predissociation depends on the quantum number N. If a $^2\Pi$ is the predissociating state, a linear dependence on J is expected. Such an effect is not observed. Moreover it is not known what features of Fig. 18 are caused by the effect of

rotation on the amount of overlap.

Gaydon's theory that the $^2\Sigma^-$ is responsible for the predissociation at low v's is appealing. Conceivably his theory holds when the $^2\Sigma^-$ is repulsive and cuts the $A^2\Sigma^+$ curve near $v = 2$ at $r > r_e$. The same $^2\Sigma^-$ could then cut $A^2\Sigma^+$ again near $v = 5$ at $r < r_e$ causing the strong predissociation.

Recently Michels and Harris (1968) have calculated potential curves for OH. They find that $^4\Sigma^-$, $^2\Sigma^-$ and $^4\Pi$ are all repulsive with $^4\Sigma^-$ cutting $A^2\Sigma^+$ near $v = 2$, $^2\Sigma^-$ near $v = 3$ and $^4\Pi$ near $v = 4$.

In summary, we have not been able to decide which state is responsible for the strong predissociation at high v's in the $A^2\Sigma^+$ state, nor if both predissociations observed in the A state are cuased by the same state.

Michel (1957) observed a sudden decrease in intensity in the (1,8) band of the $C^2\Sigma^+ \rightarrow A^2\Sigma^+$ system beginning at N = 9 and suggested that a predissociation of the A state occurs near v = 8. We agree with his findings for the $C \rightarrow A$ system and found the same effect in the $B \rightarrow A$ system. However, the same sudden intensity decrease remained in the $C \rightarrow A$ system when the bands were photographed on a much faster instrument than the high resolution spectrograph, but many higher rotational levels appeared in the $B \rightarrow A$ system. Thus the intensity drop is due to the C state rather than the A state. Moreover the intensity distribution depends very much on the way OH is formed from water. Michel (1957) also formed OH from water. We thus recommend caution in the interpretation of these intensity anomalities.

Referring to the (0,8) band of OH shown in Plate III, $R_1(4)$ or the longer wavelength component of R(4) is weaker

than it should be, by comparison to the components of R(3), R(5) and R(6); $R_1(5)$ appears fuzzy. $P_1(6)$ also also shows the abnormal intensity but the two components of P(4) and P(5) are quite normal. We are unable to explain these small perturbations, except that they are due to the upper, or B state.

Chapter X - The $C^2\Sigma^+ \rightarrow B^2\Sigma^+$ System

The $C^2\Sigma^+ \rightarrow B^2\Sigma^+$ System has never been observed previously, but its transitions can be predicted exactly from table 14. In fact the (0,0) transition of the $C \rightarrow B$ was found and the frequencies are given on table 15. It is easy to verify from combination relations that the assignment is correct. The (0,0) band of OH, although about 10 times weaker than the (0,6) band of the $B \rightarrow A$ system, appears in a clean region and was quickly identified from its structure. The heads of other bands predicted by table 14 have been observed. Even the (1,1) band of the OD system has been found at its predicted frequency. There is thus no doubt about the v numbering in the C state and about the position of the C state in the energy level diagram.

N	R_1	R_2	P_1	P_2
0	19865.75			
1	19871.20	19870.89	19845.24	
2	19876.51	19875.56	19834.39*	
3	19879.70	19876.51	19820.25	19818.48
4	19881.96	19878.94	19805.47	19804.23+
5			19789.43	19786.31

N	$\Delta_2' F_1$	$\Delta_2' F_2$	$\Delta_2'' F_1$	$\Delta_2'' F_2$
1	25.96	25.63	31.36	
2	42.12	41.17	50.95	52.41
3	59.45	58.03	71.04	71.33
4	76.49	74.71	90.27	90.20

*A hydrogen line occurs at the predicted value of the other P (2) component. The line quoted is probably $P_1(2)$.

+This line blends with an iron standard line.

Table 15. The (0,0) band of the $C^2\Sigma^+ \longrightarrow B^2\Sigma^+$ system of OH.

Chapter XI - What now OH?

This chapter discusses problems which have arisen from the research on the OH molecule and which are not resolved.

The exact size of the dispersion hump in the A state should be measured. This can be done by detecting predissociation by rotation in the $A^2\Sigma^+$ state of OD. With just slightly more extensive data than that presented here, it is very possible to see this effect. The details are given in Appendix V. The same result can be obtained theoretically since the interactions are very well known and existing computer calculation of atomic wave functions are reasonably good.

The details of the predissociations described in Chapter IX also have to be explained by theory.

The excitation of the OH molecule is peculiar. The intensity of the transitions in the $B \rightarrow A$ system falls to very small values beyond $N = 8$ (Fig. III). The calculated temperature of the OH molecules in the B state is well below room temperature. Excitation of $N > 8$ have been observed in the $B \rightarrow A$ system on a faster instrument than the 3.4 meter spectrograph. Czarny and Felenbok (1968) have found the same intensity distribution. In the

(0,6) band of the B → A system, they found that the rotational temperature is 130° K at low N and 350° K at high N. The temperature in the (0,0) transition of the A → X system has been measured by Carrington and Broida (1958) who obtained T = 669° K at low N and T = 2760° K at high N and by Meinel (1967) who found T = 610° K at low N and 20800° K at high N. The intensity distribution in the C → A system (plate IV) seems to be qualitatively the same. In each of these cases the OH was produced from H_2O and the peculiar intensity distribution may be a result of the mode of formation of OH. Although no quantitative results for OD exist, from plate IV, the C → A system of OD has qualitatively the same peculiar intensity pattern. In the B → A system of OD, the intensity drop is not noticeable until N = 20.

Many closely spaced lines without any obvious structure have been observed between 3900 Å and 4100 Å. The spectrum is different for the H_2O and D_2O sources. It is conceivable that these are transitions from the higher vibrational levels of the C state to the B state. The emitter of these lines is at present unknown.

The apparatus described in Chapter III with H_2O as source should yield a rich spectrum of OH in the vacuum ultra-violet. By looking at Fig. 14 one cannot help but feel that there are other deeply bound states of OH higher in energy than the C state. In any case, the $C \rightarrow A$ system will certainly appear (the tail end of it is reported here) and the $C \rightarrow X$ system will probably be observed too (Felenbok and Czarny, 1964).

One of the reasons for undertaking this project was to observe H_2O^+. Its spectrum is predicted to occur in the near infra-red. We have investigated up to 6500 Å and have not seen it. It is very strange that the hollow cathode, which supposedly brings out spectrum of ions, failed to bring out the OH^+ spectrum. We have observed the doubly ionized oxygen lines at 3754. 697 Å, 3757.239 Å, and 3759. 871 Å, whose excitation energy is 36.5 ev. Other O III lines were also seen. We don't understand why these highly excited lines from O III were observed, but OH^+ lines, whose excitation energy $\approx$ 15 ev. were not observed. Perhaps a different source should be used to detect H_2O^+.

In the $B \rightarrow A$ and $C \rightarrow A$ systems, the lifetime of the lower levels has been shown to be $\approx 10^{-11}$ seconds, which is much shorter than that of the upper state. Population inversion, one of the conditions for lasing action, occurs naturally in these systems. It would be interesting to build a chemical OH laser.

BIBLIOGRAPHY

Barrett, A. H. 1967. Science. 157, 881.

Barrow, R. F. 1956. Ark. fur Fysik, 11, 281.

Bennett, R. G. and Dalby, F. W. 1964. J. Chem. Phys. 40, 1914.

Born, M. and Oppenheimer, R. 1927. Ann. d. Physik, 84, 457

Branscomb, L. M. et al. 1958. Phys. Rev. 111, 504

Bunker, R. R. 1968. Jour. Mol. Spec. 28, 422.

Carrington, T. and Broida, H. P. 1958. Jour. Mol. Spec. 2, 273.

Charton, M. and Gaydon, A. G. 1958. Proc. Roy. Soc. (London) A 245, 84.

Coleman, C. D. et al. 1960 "Table of Wavenumbers" Vol. I. U.S. Dept. of Commerce. National Bureau of Standards.

Crosswhite, H. M. 1967 "F_e - N_e Hollow Cathode Standards". Unpublished.

Czarny, J. and Felenbok, P. 1968. Ann. Astrophys. 31, 141.

Dieke, G. H. and Crosswhite, H. M. 1948. "The ultra-violet bands of OH - Fundamental Data", Bumblebee series, report #87, Nov. 1948.

Dunham, J. L. 1932. Phys. Rev. 41, 721.

Felenbok, P. 1963. Ann. Astrophys. 5, 393.

Felenbok, P. and Czarny, J. 1964. Ann. Astrophys. 27, 244.

Gaydon, A. G. and Wolfhard, H. G. 1951. Proc. Roy. Soc. A 208, 63.

Herzberg, G. 1950. "Spectra of Diatomic Molecules", Van Nostrand Co., Inc.

Ishaq, M. 1937. Proc. Roy. Soc. A 159, 110.

Kolos, W. and Wolniewicz, L. 1965. Jour. Chem. Phys. 43, 2429

Kovacs, I. 1958. Can. J. Phys. 36, 309.

Landau, L. D. and Lifshitz, E. M. 1965. "Quantum Mechanics - non-relativistic Theory", Pergamon Press.

London, F. 1937. Trans. Far. Soc. 33, 8.

Meinel, A. B. 1950. Astrophys. J. 111, 555.

Meinel, H. 1967. Z. Naturforsch, 22a, 977.

Michel, A. 1957. Z. Naturforsch. 12a, 887.

Michels, H. H. and Harris, F. E. 1968. Int. J. Quant. Chem. Vol. II s, 21.

Moore, C. E. 1952. "Atomic Energy Levels" Vol. I, Circular 467, U. S. Dept. of Commerce, National Bureau of Standards.

Naegeli, D. W. and Palmer, H. B. 1967. J. Mol. Spec. 23, 44.

Oura, H. and Ninomiya, M. 1943. Proc. Phys. Math. Soc. Japan, 25, 355.

Palmer, H. B. and Naegeli, D. W. 1968. J. Mol. Spec. 28, 417.

Stone, J. M. 1963. "Radiation and Optics", McGraw - Hill Book Co., Inc., 260.

Tanaka, T. and Koana, Z. 1934. Proc. Phys. Math. Soc. Japan, 16, 365.

Tomkins, F. S. and Fred, M. 1951. J. Opt. Soc. Amer. 41, 641.

Van Vleck, J. H. 1929. Phys. Rev. 33, 467.

Weisner, J. D. and Armstrong, B. H. 1964. Proc. Phys. Soc. (London) 83, 31.

Wigner, E. and Witmer, E. E. 1928. Z. Phys. 51, 859.

Appendix I - The isotopic constant

The isotopic constant ρ is defined by

$$\rho = \sqrt{\frac{\mu}{\mu'}}$$

where μ is the reduced mass of OH and μ' is that of OD. From Herzberg (1950),

$$\mu = 0.948376$$
$$\mu' = 1.789403$$

Thus

$$\rho = 0.728008$$
$$\rho^2 = 0.529996$$
$$\rho^3 = 0.385841$$

Appendix II - A program for least-squares polynomial approximation.

Suppose that through the set of points (x_i, y_i), $i = 0, 1, \ldots n$, one wants to fit the polynomial

$$y_i = b_0 + b_1 x_i + b_2 x_i^2 + \cdots b_m x_i^m$$

under the condition of least square error E.

$$E = \sum_{i=0}^{n} \left(b_0 + b_1 x_i + \cdots + b_m x_i^m - y_i \right)^2$$

$$0 = \frac{\partial E}{\partial b_k} = 2 \sum_{i=0}^{n} \left(b_0 + b_1 x_i + \cdots + b_m x_i^m - y_i \right) x_i^k \quad , \quad k = 0, 1, \ldots, m$$

Let $\quad v_k = \sum_{i=0}^{n} x_i^k \quad ; \quad (vy)_k = \sum_{i=0}^{n} y_i x_i^k$

$$\therefore \quad v_0 b_0 + v_1 b_1 + \cdots + v_m b_m = (vy)_0$$

$$v_1 b_0 + v_2 b_1 + \cdots + v_{m+1} b_m = (vy)_1$$

$$\vdots$$

$$v_m b_0 + v_{m+1} b_1 + \cdots + v_{2m} b_m = (vy)_m$$

The b's can now be solved by Cramer's rule. In the program the b are replaced by B (k + 1), the number of parameters are N and the number of data points are N D A T A. The actual program used, and given in the following pages, was taken from the Library of Programs, UBC Computing Centre.

The parameters that best represent the $\Delta G(v + \frac{1}{2})$ quantities in the B state (Chapter VII) were calculated by hand and by computer. The results were the same.

The variables X and Y appear in the main program. Their DIMENSION in the main program is NDATA. The usual "CALL POLYFT (X, Y, N, NDATA)" in the main program will introduce compilation and execution of the subroutine.

FORTRAN SOURCE LIST

```
ISN       SOURCE STATEMENT

  0 # $IBFTC POLYFT
  1 #       SUBROUTINE POLYFT (X,Y,N,NDATA)
  2 #       DIMENSION X(NDATA),Y(NDATA)
  3 #       DIMENSION A(10,10), V(20), VY(11),B(10)
  4 #       DIMENSION EP(500)
  5 #       COMMON /COEFF /B
  6 #       COMMON/RMSE/E
    # C
  7 #       PRINT 323, N, NDATA
 10 #   323 FORMAT(1H-,6X,4HN = ,I3, 5X, 8HNDATA = , I3/)
    # C
    # C     BEGIN CALCULATION OF POLYNOMIAL COEFFICIENTS
    # C     N IS THE POLYNOMIAL DEGREE
    # C     NDATA IS THE NO. OF DATA POINTS
 11 #       NP1 = N+1
 12 #       NP2=N+2
 13 #       N21=2*N+1
 14 #       E=0.
 15 #       DO 100 I=1,NP2
 16 #       V(I)=0.
 17 # 100   VY(I)=0.
 21 #       DO 106 I=NP2,N21
 22 # 106   V(I)=0.
 24 #       DO 105 I=1,NDATA
 25 #       VY(1)=VY(1)+Y(I)
 26 #       VY(NP2)=VY(NP2)+Y(I)*Y(I)
 27 #       XX=X(I)
 30 #       DO 101 J=2,NP1
 31 #       V(J)=V(J)+XX
 32 #       VY(J)=VY(J)+XX*Y(I)
 33 # 101   XX=XX*X(I)
 35 #       DO 105 J=NP2,N21
 36 #       V(J)=V(J)+XX
 37 # 105   XX=XX*X(I)
 42 #       V(1)=NDATA
    # C     ABOVE BUILT UP V,NOW BUILD UP A
 43 #       DO 102 K=1,NP1
 44 #       DO 102 L=1,K
 45 #       KSL1=K-L+1
 46 # 102   A(L,KSL1)=V(K)
 51 #       DO 103 K=NP2,N21
 52 #       LS=N21-K+1
 53 #       DO 103 L=1,LS
 54 #       KLNP1=K+L-NP1
 55 #       NP2L=NP2-L
 56 # 103   A(KLNP1,NP2L)=V(K)
 61 #       DO 104 K=1,NP1
 62 # 104   A(K,NP2)=VY(K)
    # C     WE NOW SOLVE A MATRIX A OF N+1 ROWS AND NP2 COLUMNS
 64 #       DO 399 I = 1, N
 65 #       IP1=I+1
 66 #       DO 399 J = IP1,NP1
 67 #       Q=A(J,I)/A(I,I)
 70 #       DO 399 K = IP1, NP2
 71 # 399   A(J,K) = A(J,K) - A(I,K)*Q
```

FORTRAN SOURCE LIST POLYFT

```
ISN        SOURCE STATEMENT

  75 *          B(NP1)=A(NP1,NP2)/A(NP1,NP1)
  76 *          DO 301 I=2,NP1
  77 *          J=NP2-I
 100 *          JP1=J+1
 101 *          B(J)=A(J,NP2)
 102 *          DO 302 K=JP1,NP1
 103 *  302     B(J)=B(J)-B(K)*A(J,K)
 105 *  301     B(J)=B(J)/A(J,J)
 107 *          DO 398 I = 1, NP1
 110 *  398     E = E + B(I)*VY(I)
 112 *          E=VY(NP2)-E
 113 *          ESUM = 0.
 114 *          DO 333 K = 1, NDATA
 115 *          TS = B(1)
 116 *          DO 95 MM = 2,NP1
 117 *          ML = MM-1
 120 *     95   TS = TS + B(MM)*X(K)**(ML)
 122 *          EP(K) = (Y(K)-TS) * (Y(K)-TS)
 123 *    333   ESUM = ESUM + EP(K)
     * C
     * C      END CALCULATION OF POLYNOMIAL COEFFICIENTS
     * C
 125 *          NP1=N+1
 126 *          PRINT 310,(K,B(K),K=1,NP1)
 133 *    310   FORMAT (7X, 2HB(I1,2H)=F12.5)
 134 *          XN = NDATA
 135 *          E = SQRT (ESUM/XN)
 136 *          PRINT 340,E
 137 *    340   FORMAT(1H0,10X,24HLEAST SQUARES ERROR    = ,F12.5)
 140 *          RETURN
 141 *          END
```

NO MESSAGES FOR ABOVE ASSEMBLY

Appendix III - Zero point Energy.

Knowledge of ω_e and $\omega_e x_e$ for a molecule means that G (0) can be determined since

$$G(0) = \frac{\omega_e}{2} - \frac{\omega_e x_e}{4}$$

The minimum of a potential curve can then be determined. The following table gives these values for several electronic states of OH and OD.

State	OH	OD
$X\ ^2\Pi$	1846.9 3.14	1349.4 2.58
$A\ ^2\Sigma^+$	1566.5 2.58	1140.7 1.60
$C\ ^2\Sigma^+$	611.7 -0.99	447.0 * -0.50 *

On the bottom line is given the Dunham zero point correction term Y_{oo},

$$Y_{oo} = \frac{B_e}{4} + \frac{\alpha_e \omega_e}{12 B_e} + \frac{\alpha_e^2 \omega_e^2}{144 B_e^3} - \frac{\omega_e x_e}{4}$$

* From isotopic relations.

Appendix IV - Thermal broadening and Pressure broading of Spectral Lines.

Some spectral lines in the spectrum of OH and OD were observed to be broad. The increased breadth is not due to thermal broadening nor pressure broadening because transitions from the same upper state were observed to be broad and sharp (in OH, the (1,4) and (1,9) transitions are sharp, but (1,5) and (1,6) are broad). Nevertheless, the classical line breadth due to temperature and pressure can be calculated. According to Stone (1963) "Radiation and Optics", the half width of a spectral line is given by

$$\Delta = \frac{2\omega_o}{c}\left(\frac{2kT}{M}\right)^{1/2}$$

where ω_o is the frequency of the transition

c is the speed of light $= 3 \times 10^{10}$ cm/sec

k is Boltzmann's constant $= 1.4 \times 10^{-16}$ erg/deg

T is the temperature $\approx 330°$ K

M is the mass of the molecule

For $\lambda = 4000$ Å and for molecular hydrogen ($M = 2 \times 1.7 \times 10^{-24}$ gm),

$$\Delta = 2.5 \times 10^{10} \text{ / sec.}$$

This is only a factor of 10 less than that due to predissociation. In fact, several H_2 lines were identified and they are all sharp.

From Stone, the half width of a spectral line due to pressure broadening is

$$\gamma = \frac{8\sqrt{\pi}\, D^2 P}{(M k T)^{1/2}}$$

where D is the diameter of the molecule and P is the pressure. The maximum pressure is that of H_2O at 50° C which is 95 mm Hg. Taking $D^2 = 10^{-16}$ cm^2, then for H_2

$$\gamma = 240 \text{ / sec.}$$

Thus collisions in the classical sense do not contribute at all to the half width. As long as the effective diameter of the molecule is less than 10^4 Å, collisions are not important.

Appendix V - Predissociation by Rotation in the $A^2\Sigma^+$ state of OD

The magnitude of the dispersion hump in the A state could be determined if predissociation by rotation were observed in the $A^2\Sigma^+$ state of OD. From table 14, the v = 13 level is 114 cm^{-1} from the expected limit, v = 12 is 548 cm^{-1}, v = 11 is 1284 cm^{-1}, v = 10 is 2172 cm^{-1} and v = 9 is 3290 cm^{-1}. From the B_v values, it is expected that, excluding rotation, N = 8 levels are bound in v = 13, N = 12 in v = 12, N = 17 in v = 11, N = 20 in v = 10 and N = 24 in v = 9. The N = 18 level has been seen in v = 11 (0,11 transition) and N = 21 in v = 10 (0, 10 transition). It is thus quite possible that predissociation by rotation can be detected in the $A^2\Sigma^+$ state of OD with little modification of the technique described in the thesis.

Appendix VI - Electronic isotope effect

The accuracy of the dissociation energy of the $A^2\Sigma^+$ state of OH and OD, as presented in this thesis is just outside the range of detecting electronic isotope shifts. This effect arises from the difference in the shape of the potential well for two molecules, of different isotope, e.g. OH and OD. Imagining the molecule to be neither vibrating nor rotating, the electronic motion is still present since the molecule is held together by the electrons. The electrons in turn drag the nuclei behind them. Because the center of mass is different for OH and OD, the energy to "keep the molecule at minimum" of the potential is different for OH and OD. Mathematically, this effect is due to the breakdown of the Born-Oppenheimer approximation. Bunker (1968) has calculated electronic isotope shifts in several molecules and they are typically of the order of $5\sim10$ cm^{-1}. The agreement of his theory with experiment is not bad.

For OH, Bunker's formula predicts that OH potential wells are deeper than the OD potential wells by 6.7, 51.1, - 0.7 and 4.50 cm^{-1} in the X, A, B and C states respectively.

Experimentally, we have obtained $(5.8 \pm 15)\ cm^{-1}$ and $(-3.6 \pm 15)\ cm^{-1}$ for the X and A states respectively.